SYNTHESIS AND MODIFICATION OF ALUMINA NANOFIBRES AND ITS APPLICATOINS

Yiming Huang

Master of Applied Science

Submitted in fulfilment of the requirements for the degree of

Master of Applied Science

Faculty of Science and Engineering

Queensland University of Technology

Feb. 2013

Keywords

Boehmite nanofibres, γ-Alumina nanofibres, hydrothermal synthesis, enzyme immobilisation, covalent bonding, physical adsorption, silane, surface modification, protein cross-linking, ultra-filtration membrane, surface modification, hydrophobicity, dextran retention, water flux and protein separation.

Abstract

This thesis describes two optimised synthesis methods of Alumina Nanofibres, the characterisation techniques and results are displayed, and two applications of synthesised Alumina Nanofibres are presented.

In the first application of enzyme immobilisation, the Alumina Nanofibres are functionalised with (3-aminopropyl) triethoxysilane (APTES) group and covalently connected to Laccase using the cross-linking agent Glutaraldehyde (GA). The immobilisation condition has been optimised and compared with physical adsorption in respect to speed and concentration. After the immobilisation process, the activity of Laccase is retained to a great extent when compared to free Laccase. The catalytic activity of immobilised Laccase is tested using 2,2'-Azinobis-(3-tehylbenzthiazoline-6-sulphonate) (ABTS) method and results indicate immobilisation have positive impact on resistance to pH and temperature change. In the reusability test, the covalent immobilisation strategy exhibits better performance in continuous cycle reaction test comparing to physical adsorbed laccase.

Large-scale purification/separation of bio-substances is a key technology required for rapid production of biological substances in bioengineering. Membrane filtration is a new separation process and has potential to be used for concentration (removal of solvent), desalting (removal of low molecular weight compounds), clarification (removal of particles), and fractionation (protein-protein separation). In this study, the Alumina Nanofibres are dip coated on top of a porous support to form a separation layer to develop an efficient membrane for protein separation. The

radical changes in membrane structure provided new ceramic membranes with a large porosity (more than 70%) due to the replacement of bulk particles with fine fibers. The pore size had an average of 11 nm and pure water flux was approximately 400 $L \cdot h^{-1} \cdot m^{-2} \cdot bar^{-1}$. The surface of membrane is further modified by (3-aminopropyl) triethoxysilane (APTES), the filtration property was enhanced due to the surface hydrophobic conversion. The water flux of modified membrane reduced dramatically whereas the protein separation efficiency improved significantly. The molecular cut-off of the membrane is measured by filtrating standard dextran solution of different molecular mass. The final silane-grafted alumina fiber membranes were demonstrated to reject 100% BSA protein and 92% cellulase. It was also able to retain 75% trypsin and maintain a permeation flux of 48 $L \cdot h^{-1} \cdot m^{-2} \cdot bar^{-1}$.

Table of Contents

Keywords i
Abstract ii
Table of Contents iv
List of Figures vi
List of Abbreviations ix
Statement of Original Authorship ..... **Error! Bookmark not defined.**
Acknowledgements xi
CHAPTER 1: INTRODUCTION TO ALUMINA NANOFIBRES ..... - 1 -
1.1 Introduction ..... - 1 -
1.2 Synthesis and Characterisation of Alumina Nanofibres ..... - 1 -
1.2.1 Synthesis of Alumina Nanofibres ..... - 1 -
1.2.2 Characterisation of Alumina Nanofibres ..... - 3 -
CHAPTER 2: IMMOBILISATION OF LACCASE ON FUNCTIONALISED ALUMINA NANOFIBRES ..... - 4 -
2.1 Introduction ..... - 4 -
2.2 Experimental ..... - 8 -
2.2.1 Materials ..... - 8 -
2.2.2 Preparation of Alumina Nanofibres (Al-Fibre) ..... - 9 -
2.2.3 Preparation of Amino Silane Functionalised Alumina nanofibres (NH-Fibre) ..... - 10 -
2.2.4 Preparation of GA Bonded Alumina Nano-fibre (GA-Fibre) ..... - 10 -
2.2.5 Immobilisation of Laccase on Functionalised Alumina Nanofibres ..... - 11 -
2.2.6 Enzymatic Activity Determination ..... - 12 -
2.2.7 Resistance to pH Value and Temperature Change ..... - 12 -
2.2.8 Reusability of Immobilised Laccase ..... - 13 -
2.2.9 Characterisation ..... - 14 -
2.3 Results and Discussion ..... - 15 -
2.3.1 Characterisation of Supports ..... - 15 -
2.3.2 Immobilisation of Laccase ..... - 19 -
2.3.3 Activity of the Immobilised Laccase ..... - 22 -
2.3.4 Resistance to pH value and Temperature ..... - 23 -
2.3.5 Reusability ..... - 26 -
2.4 Conclusion ..... - 26 -
CHAPTER 3: MODIFIED ALUMINA NANOFIBRES COATING ON POROUS ALUMINA SUPPORT FOR PROTEIN SEPARATION ..... - 28 -
3.1 Introduction ..... - 28 -
3.2 Experimental ..... - 33 -
3.2.1 Materials ..... - 33 -
3.2.2 Fabrication of Surface Functionalised Alumina Nanofibres Membrane ..... - 34 -
3.2.3 Performance of Ultra-filtration Membrane ..... - 37 -

3.2.4 Characterisation Techniques and Instruments.....- 38 -
3.3 Results and Discussion .....- 42 -
3.3.1 Effect of Temperature on the Synthesis of Boehmite Nanofibres .....- 42 -
3.3.2 Effect of Reaction Time on the Synthesis of Boehmite Nanofibres ...- 43 -
3.3.3 Characterisation of Boehmite Nanofibres and Ultra-filtration Membrane.....- 45 -
3.3.4 Performance of Ultra-filtration Membrane .....- 51 -
3.4 Conclusion .....- 59 -
CHAPTER 4: CONCLUSION AND FUTURE PROSPECTIVE.....- 61 -
4.1 Laccase Immobilisation on Functionalised Alumina Nanofibres.....- 61 -
4.2 Functionalised Alumina Membrane for Protein Separation .....- 62 -
BIBLIOGRAPHY ..... - 64 -

List of Figures

Figure 2.1 Mechanism of Protein Attachment on Functionalised Alumina Nanofibres	7
Figure 2.2 Wide-angle XRD patterns of 3 different supports before laccase immobilisation	16
Figure 2.3 TEM image of Alumina nanofibres	17
Figure 2.4 IR spectra of the functional group attached Al-Fibre.	19
Figure 2.5 (a) Immobilised amounts of laccase on the supports as a function of time. (b) Immobilised amounts of laccase on the supports as a function of laccase concentration. (c) Zeta potential vs pH value of Laccase and NH-fibre.	21
Figure 2.6 Resistance of pH value and temperature comparison between Free Laccase and Immobilised Laccase.	23
Figure 2.7 Activity of the free and immobilised laccase at different pH values.	24
Figure 2.8 Activity of the free and immobilised laccase at different temperature	24
Figure 2.9 Reusability of laccase on NH-Fibre and GA-Fibre.	25
Figure 3.1 Alumina disc support	36
Figure 3.2 TEM images of Boehmite nanofibres as effect of reaction temperature. (a) Boehmite nanofibres synthesized at 130℃. (b) Boehmite nanofibres synthesized at 180℃.	43

Figure 3.3 TEM images of Boehmite on effect of reaction time. (a) Boehmite nanofibres synthesized in 12 hours. (b) Boehmite nanofibres synthesized in 24 hours. (c) Boehmite nanofibres synthesized in 48 hours. (d) Boehmite nanofibres synthesized in 72 hours. 44

Figure 3.4 N^2 adsorption result of three nanofibres of different reaction time. 46

Figure 3.5 (a) Thermo-gravimetry of Boehmite nanofibres (TG), (b) Derivative Thermo-gravimetry (DTG) of Boehmite nanofibres. 47

Figure 3.6 XRD patterns of Boehmite nanofibres, Original disc support and Boehmite nanofibres coated support. 48

Figure 3.7 FESEM image of Alumina nanofibres coated disc support and SEM image of blank support. 49

Figure 3.8 The image of water droplets on NH-membrane 50

Figure 3.9 The FTIR spectra of Al-membrane, Silane(ApTES) and NH-membrane 51

Figure 3.10 Water flow rates through membranes as a function of applied pressure: (a) a porous α-alumina support; (b) a γ-alumina fiber membranes and (c) a silane-grafted fiber membrane. 53

Figure 3.11 Molecular retention curves of support, Bo-Membrane, Al-Membrane and NH-Membrane. 55

Figure 3.12 Protein separation efficiency of membrane. (a) BSA separation efficiency of membranes, (b) Cellulase separation efficiency of membranes, (c) Trypsin separation efficiency of membranes. (d) The protein separation efficiency of *NH-membrane* 58

.

List of Abbreviations

ABTS	2,2'-Azinobis-(3-tehylbenzthiazoline-6-sulphonate)
Al-fibre γ-	Alumina nanofibres
APTES	(3-aminopropyl) triethoxysilane
ATR-SEIRAS	applied surface enhanced infrared adsorption spectroscopy
BET	Brunauer-Emmett-Teller
BSA	albumin from bovine serum
DTG	thermo-gravimetry
GA	glutaraldehyde ,
GA-Fibre	glutaraldehyde and APTES grafted Alumina nanofibres
GPC	gel permeation chromatography
IR	infrared spectroscopy
M.W	molecular weight
MWCO	molecular weight cut off
NH-Fibre	APTES grafted Alumina nanofibres
NH-Membrane	Alumina disc support coated with APTES grafted Alumina nanofibres
PBS	phosphate buffer solution
TEAOH	tetraethyl ammonium hydroxide solution
TG	thermo-gravimetry
UV-Vis	ultraviolet-visible spectroscopy
WAXRD	wide-angle X-ray diffraction

Statement of Original Authorship

The work contained in this thesis has not been previously submitted to meet requirements for an award at this or any other higher education institution. To the best of my knowledge and belief, the thesis contains no material previously published or written by another person except where due reference is made.

Signature: 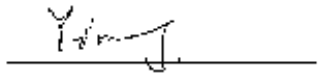

Date: 29/08/2013

Acknowledgements

I would like to offer my appreciation to those who provided assistance to my work for the past two years, this thesis would not have been possible without their contribution.

First and foremost, I would like to express my sincere gratitude to my supervisors, Prof. Huaiyong Zhu and Dr. Xuebin Ke, for their patient guidance, support, encouragement and scientific knowledge they shared with me.

I'm also grateful to Dr. Zheng for his advises and helping with TEM. My gratitude extends to other research group members: Jane Zhao, Mark Zhang, Sarina Sarina, Sifani, Kelvin Xiao, Arixn Bo and Chen Chao, for their valuable research advice and collaboration

In addition, I would like to thank Dr. Wayde Martens, Dr. Llew Rintoul, Dr. Chris Carvalho and Dr. Tim Dargaville for their knowledge and training of instruments technology, and also to many other technicians of chemistry for their assistance in the daily work.

I would like to acknowledge the Central Analytical Research Facility for use of the facilities, especially to Dr. Peter Hine, Dr.Hui Diao and Dr. Tony Raftery for their assistance with SEM and XRD technology.

I wish to extend my appreciation to my fellow postgraduate students and the colleagues of the Faculty of Science and Engineering, for the friendly environment.

Finally, I would like to acknowledge my parents for their forever love, support and understanding.

Chapter 1: Introduction to Alumina Nanofibres

1.1 INTRODUCTION

Nano-structured materials have attracted much attention in the past few decades because of their novel physical and chemical properties compared to their corresponding bulk materials. The nano materials and corresponding nanotechnology have found enormous and significant applications in physical, chemical and biology areas.

Alumina nanomaterial is of particular interest and is currently being extensively studied. Alumina nanomaterial nanostructures range from 0-dimensional quantum dot to 3-dimensional matrix. Among which, the one-dimensional nanomaterials known as nanorods, nanoribbons, nanotubes, nanofibres, nanowires and nanowhiskers simply based on their morphology are of most interest for its applications in advanced catalysts, adsorbents, composite materials and ceramics[1][2][3]. In this thesis, we focused on the Alumina nanofibres: synthesis method and applications in catalysts and membranes.

1.2 SYNTHESIS AND CHARACTERISATION OF ALUMINA NANOFIBRE

1.2.1 Synthesis of Alumina Nanofibres

One-dimensional nanomaterials were discovered to be generated on the interface of different state phases, using synthesis methods such as vapour-liquid-solid ,vapour-solid and liquid-solid processes [4] [5] [6].

Among all these possible synthesis strategies, Alumina nanofibres were mostly fabricated through solution based hydrothermal reactions, based on research by Bugosh who reported the preparation of fibrous colloidal boehmite, the precursor of Alumina material [7]. In 2006, Shen's group developed another boehmite nanofibres synthesis path by a wet-gel conversion assisted by water vapour. In the method, aluminium nitrate $Al(NO_3)_3$ was mixed with NH_4OH to form a wet-gel cake, the wet-gel was heated to 200℃ in the presence of steam to create boehmite nanofibres with diameter of 20-30 nm and length of 100-400nm[2]. Three years later, they changed NH_4OH to tetraethylammonium hydroxide (TEAOH) keeping all other conditions the same, and this time they obtained nanofibres of 200-400nm length and 15-20nm thick. Moreover, Kuiry successfully synthesised boehmite nanofibres using Aluminium isopropoxide, resulting in 10μm long and 120nm thick Boehmite nanofibres [1].

In addition to the work by Shen and Kuiry, other researchers found that surfactant would act as a template reagent during the boehmite nanofibres synthesis process. For instance, Zhang tested the effect of a series of Pluronic surfactants in the boehmite preparation and explained the mechanism of the surfactant template by comparing the resultant boehmite nanofibres with different Al/surfactant molar ratios [6] . Lee employed both cationic and non-ionic surfactants into the aluminium tri-sec-butoxide, the results indicated that non-ionic surfactant is beneficial to the growth of boehmite nanofibres where the length of 180nm and diameter of 18nm were observed. In contrast, the boehmite nanofibres synthesised with cationic surfactant exhibited only 3nm diameter and 20nm length [8].

In the previous work of our group [9], boehmite nanofibres are generated by hydrothermal reaction of a mixture of sodium aluminate $NaAlO_2$ and acetic acid in the presence of Polyethylene oxide (PEO) surfactant at 100℃ for a period of 48 hours, resulting in boehmite nanofibres with length greater than 50nm and thickness of 3nm. Then, we adjusted the Al/surfactant molar ratio and the synthesis period from 2 to 8days, and found that the longest nanofibres with length 92nm and diameter 5.2nm was achieved [10].

In this thesis, the formation of boehmite nanofibers is optimised on the basis of our previous work, the synthesis period was reduced to 2 days while the obtained boehmite nanofibres was 100-120nm in length and 10nm in diameter.

1.2.2 Characterisation of Alumina nanofibres

A range of characterisation techniques has been used to characterise the properties of Alumina nanofibers. The morphology is provided by Scanning electron microscope (SEM) and Transmission electron microscopy (TEM), while X-ray diffraction is utilised to obtain crystal information. Surface area of Alumina nanofibres is calculated by Nitrogen adsorption results using the Brunauer-Emmett-Teller (BET) equation. Thermal gravimetric analysis along with the differential thermal analysis provides information on phase transformation.

Chapter 2: Immobilisation of Laccase on Functionalised Alumina Nanofibres

2.1 INTRODUCTION

Laccase (Benzenediol oxygen oxidoreductase, E.C. 1.10.3.2) is a series of enzymes firstly discovered at the end of the 19^{th} century and then found in various organisms such as bacteria [11], fungus, plants, and insects [12]. Extensive studies on laccase have been conducted since it was found to play a crucial role in the both lignin synthesis and degradation processes [13]. In these processes, the copper centre of laccase, contains of four copper atoms in the 2^{+} oxidation state, accelerate the removal of an electron from Phenolic hydroxyl to generate free Phenoxy radicals [14] [15] [16]. Due to its extraordinary catalytic suitability, laccase is widely applied in textile industry, food industry, paper industry and environmental field [17] [18] [19] [20] [21] [22] [23]. However, the high solubility of laccase in water makes it difficult to separate out from the substrate and products and consequently hard for re-utilisation. In addition, the denaturation of laccase under extreme pH and temperature condition results in not a desirable trait. These two main disadvantages are the major obstacles of laccase for large-scale practical applications.

Immobilisation of laccase at insoluble material surface is found to be a proven effective and straightforward strategy for practical utilisations [24] [25]. Once immobilised on insoluble supports, laccase can be converted to heterogeneous catalysts which exhibit remarkably improved stability and reusability compared to free laccase [26]. As a consequence, enormous efforts have been made in laccase immobilization strategy, during which several immobilisation methods have been reported and various types of materials as well as their modifications have been successfully applied [27] [28]. First of all, there are two basic methods for immobilisation: physical adsorption and covalent bonding, comparing to the former one, the covalent bonded laccase shows significant better stability due to the stronger attachment which is crucial for the reutilisation [29] [30]. For example, covalently bonded laccase on the functionalised polymer support presented extraordinary reusability in the repeat remediation of waste materials treatment [31]. On the other hand, researchers never stop looking for better materials as immobilisation supports. For instance, Pita and Gutierrez-Sanchez covalently attached laccase onto gold by modifying the gold surface with a mixed monolayer of an aromatic diazonium salt derivative and 6-mercapto-1-hexanol as covalent linkage [32]. Vaz-Dominguez and Pita continued this work and applied surface enhanced infrared adsorption spectroscopy (ATR-SEIRAS) and scanning tunnelling microscopy (STM) to further investigate the immobilisation of laccase on chemically modified gold electrodes [33]. Despite gold electrodes, nanoporous gold was employed by Qiu and Xu, they focused on different immobilisation strategies and corresponding particle size effects [34]. Mesoporous silica sphere is another commonly used material for laccase immobilisation, for example, Zhu and Kaskel prepared mesoporous silica spheres and then magnetic nano particles were loaded. As a result, newly designed catalysts

can easily be separated by magnetic field so that damages caused by mechanical separation can be avoided [35]. Liu and Zeng completed a similar work to Zhu and Kaskel's, in which mesoporous silica spheres were changed to mesoporous carbon material. Addition to inorganic materials, researchers also developed laccase immobilization strategy on organic and bio-materials [36]. Among which, polymer fibres attracted the earliest attention, for example Wang and Peng coated oxygen plasma on PMMA/O-MMT micro-fibrous membranes to create better adsorbent for laccase immobilisation [37]. On the other hand, Bayramoglu along with Yilmaz focused on functionalised bio-membrane materials, they turned chitosan membrane into epoxy-functionalised chitosan beads to create novel high efficient immobilisation supports. In the following year, Bayramoglu and Gursel immobilised laccase on a biopolymer support: itaconic acid grafted and Cu (II) ion chelated chitosan membrane [38] [39]. In another interesting research, Moccelini and Franzoi not only fabricated immobilised laccase on biopolymer substrate-cellulose acetate, they also extended its application to biosensors [40].

Alumina nanofibre support is a kind of novel material well known as support for heterogeneous catalyst, however to the best of my knowledge, immobilisation of laccase on alumina nanofibres has not been investigated yet. First advantage of alumina nanofibre is the large surface area of nanofibre structure which is essential to the immobilisation capacity. Secondly, Alumina nanofibres along with the attached catalyst can be simply separated by centrifugation for reutilisation. Furthermore, comparing to other reported support materials, gold plate for instance, alumina nanofibres are low cost and easily synthesized, they have no chemical interaction with bio-molecular while heavy metal or its ion could causes irreversible

denaturation in many cases. In addition, organic membrane blended by polymer fibre material, which is another commonly reported support, is could have interaction with organic solvent and sometimes it participates in catalytic reactions and causes side products. In the contrary, alumina material is noble to organic regent under mild condition.

In this study, reported is an immobilised laccase system supported by (3-aminopropyl) triethoxysilane (APTES) functionalised alumina nanofibres (NH-Fibre) [41]. Laccase was attached on Alumina nanofibres through covalent bonding strategy. As shown in Figure 2.1, the functional silane group was firstly grafted on the surface of alumina nanofibre owing to Al-O-Si bond. Then the cross-linking agent Glutaraldehyde (GA) was employed to connect the -NH_2 end of APTES and the amino end of laccase [42] [43]. In addition to covalent bonded laccase, the physical adsorption of laccase on NH-Fibre was also tested and designed as a comparison. The immobilisation capacity was studied with two impact parameters, the catalytic activity of immobilised laccase was determined with free laccase, physical absorbed laccase and covalently bonded laccase.

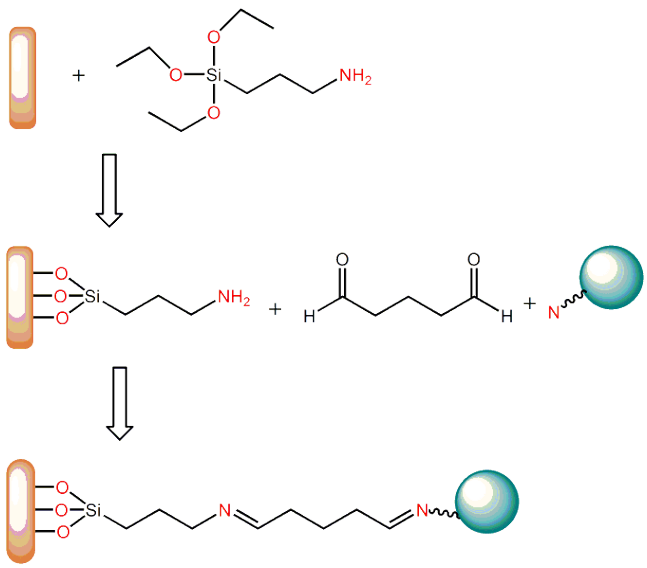

Figure 2.1Machenisam of Protein Attachment on Functionalised Alumina Nanofibres

The activity of laccase could be examined with several specific substrates [44], in this study, 2, 2'-azinobis (3-ethylbenzthiazolin-6-sulfonate) (ABTS) method was selected for the activity evaluation [45], in which ABTS was converted to green cation radicals ($ABTS^{\cdot+}$). The quantity of $ABTS^{\cdot+}$ product could easily be measured by UV-Vis spectroscopy [46], and the catalytic activity was defined by the converting speed. The thermal and pH stability of immobilised laccase system have been investigated and compared to the free enzyme. The reusability of covalent bonded laccase was tested in a continuous cycle reaction, the result was compared to physical adsorbed laccase in order to demonstrate the advantage of using covalent bonding immobilisation method.

2.2 EXPERIMENTAL

2.2.1 Materials

Unless otherwise stated, all the chemicals used were commercially purchased from suppliers and used without any further purification. The enzyme Laccase from *Trametes versicolour*, Glutaraldehyde (GA), (3-aminopropyl) triethoxysilane (APTES) 2,2'-Azinobis-(3-tehylbenzthiazoline-6-sulphonate) (ABTS), 25% Tetraethylammonium hydroxide solution (TEAOH) and Aluminium nitrate ($Al(NO_3)_3 \cdot 9H_2O$) were purchased from Sigma-Aldrich. ABTS solution was freshly prepared and applied within 24 hours since it is sensitive to visible light. Phosphate buffer solution (PBS) of wide pH value range was prepared by sodium dihydrogen

phosphate (NaH_2PO_4), disodium hydrogen phosphate (Na_2HPO_4), monopotassium phosphate (KH_2PO_4) and Citric acid . All other chemicals used in the experiment were of analytical grade.

2.2.2 Preparation of Alumina nanofibres (Al-Fibre)

Alumina nanofibres were synthesized following a previously reported method [47] [2]. In this method, boehmite nanofibres, the precursor of Alumina nanofibres, were synthesised and then transferred to γ-phase Alumina by calcination. In the synthesis procedure, firstly 30g of 25% $Al(NO_3)_3 \cdot 9H_2O$ was dissolved in 100ml deionised water and kept stirring for 1.5 hours to form a homogenous solution at room temperature. Then, 25% TEAOH was drop-wisely added into a $Al(NO_3)_3$ solution until the pH value was stabilised at 5.0. The adjustment of pH value is crucial to ensure boehmite nanofibre structure form. The white precipitates were recovered by vacuum filtration and then transferred into autoclaves, in which the precipitates were physically separated from 2ml of water and kept at 170 ℃ for a period of 72hr. The collected boehmite nanofibres were washed with deionised water three times and once with ethanol, washed nanofibres were recovered using a centrifuge (4000rpm) and dried in air at 60℃ overnight. Lastly, prepared boehmite nanofibres were calcined at 550℃ for a period of 10 hours to completely convert to γ-phase Alumina nanofibres.

2.2.3 Preparation of Amino Silane Functionalised Alumina Nanofibres (NH-Fibre)

Alumina nanofibres were grafted with silane to activate the surface of Alumina for further fictionalisation. In this work, APTES which possess an amino end was selected as the coupling agent to functionalize Al-Fibre, the silane group was attached by the method of refluxing the suspension containing Alumina nanofibres, APTES and toluene [48]. In this experiment, 3g Al-Fibre was dispersed in 100ml absolute anhydrous toluene, to the suspension 1.8g of APTES was added. The above mixed suspension was heated to 110℃ in oil bath with refluxing device and kept stirred for a period of 36 hours. Grafted Al-Fibre were recovered by centrifuge (4000rpm) and rinsed with absolute ethyl alcohol 3 times to remove un-reacted APTES and then dried in air at 60℃. Collected products were denoted as NH-Fibre.

2.2.4 Preparation of GA Bonded Alumina Nano-fibre (GA-Fibre)

The APTES grafted Alumina nanofibres was not completely ready for protein attachment yet, a cross link agent was required between enzyme molecular and the amino end of APTES group. Therefore, NH-Fibre was designed to couple with the cross-linking agent GA which is a commonly applied bridging agent for the connection of target proteins [24]. In this experiment, 300mg of NH-Fibre was dispersed in 30ml pH7.0 buffer solution, the suspension was ultra-sonicated for 10mins for better dispersion. To such dispersion, 0.5ml of GA liquid was mixed into,

the mixed dispersion was gently stirred for a period of 1 hour. The GA-Fibre was obtained from the fully engagement of NH-Fibre and GA molecular, it was washed with deionised water 3 times and recovered by centrifuge (4000rpm), the product was dried and stored in vacuum in order to isolate from oxygen.

2.2.5 Immobilisation of Laccase on Functionalised Alumina Nanofibres

The enzyme laccase was covalently bonded on GA-Fibre following steps below: certain amount of laccase powder was dissolved in 10ml of pH7.0 buffer solution, to this solution 25mg of GA-Fibre was dispersed. The dispersion was placed on shaking bed for a certain period at room temperature. The immobilised laccase was separated by centrifuge from laccase solution (2000rpm 5mins) and resined with deionised water. For comparison, Al-Fibre and NH-Fibre support was applied in parallel experiments following the exact same procedures, the laccase was physically adsorbed by these two supports.

The immobilisation capacity of supports was determined by calculating the difference between concentration of original laccase solution and residue solution. The laccase concentration was determined by measuring the Uv-Vis adsorption at 280nm and comparing the adsorption to standard curve.

In order to study the immobilisation capacity of alumina nanofibre supports, the immobilisation process was investigated with two factors: concentration of original laccase solution and immobilizing period. In the first experiment, supports were dispersed in pH 7.0 laccase solution with concentration ranging from 0-800ppm, the immobilisation period was set as 12 hours for guaranteed equilibrium adsorption. In

the other experiment, alumina supports were dispersed in the pH 7.0 laccase solution with 1000ppm concentration, the immobilisation period setting was ranged from 5mins to 480mins.

2.2.6 Enzymatic Activity Determination

ABTS is a compound commonly used to study the reaction kinetics of multi-copper oxidise enzymes including laccase. It was employed as substrate in the laccase activity test due to the phenomenon driven by laccase that the transformation from ABTS to radical cation $ABTS^+$ [34]. In this particular reaction, ABTS was selectively transferred to $ABTS^{+\cdot}$ a kind of green cation radical which has identifiable UV-Vis absorption peak at 420nm. The UV-Vis absorption tests were conducted within 20mins after reaction. The concentration of $ABTS^+$ could be calculated by equation as below:

$$C = \frac{A}{\varepsilon \cdot b}$$

Where C is the concentration of $ABTS^+$ in mol/L, A is the UV-Vis absorption, the absorptivity $\varepsilon=3.6\cdot10^4\ M^{-1}\cdot cm^{-1}$, b is the thickness of cuvette in cm.

In this project, 1 unit of laccase activity corresponds to the amount of laccase which convert 1μmol ABTS to $ABTS^+$ per minute.

2.2.7 Resistance to pH Value and Temperature Change

The resistance strength to pH and temperature change is an essential property of both free enzyme and immobilised laccase [49]. The activity of the free and immobilised laccase was tested at 25℃ with different pH value (3.0-7.0) buffer solution, which is constituted by NaH_2PO_4-Citric acid buffer system, in order to determine the resistance of laccase to pH changes. The laccase activity at pH value 4.0 was set as 100%. On the other hand, in order to determine the resistance of laccase to temperature another similar experiment was conducted at pH value 4.0 but temperature ranging from 10℃ to 80℃. The laccase activity at 50℃ was set as 100%.

2.2.8 Reusability of Immobilised laccase

Reusability is another important property of immobilised enzyme which indicates the bonding strength between supports and laccase. In this section, covalently immobilised laccase was applied in a routine activity test and then was separated from solution by 2000rpm centrifuge and washed with pure water for 3 times to remove substrate and product. Then the recovered immobilised laccase was applied to another routine activity test immediately to determine the reusability of loaded laccase. One routine activity test was recorded as 1 cycle, 10 cycles of reaction was conducted constantly in this section. For comparison, the above procedures were repeated using laccase which physically adsorbed by NH-Fibre.

2.2.9 Characterisation

2.2.9.1 X-ray Diffraction

The wide-angle X-ray diffraction (WAXRD) patterns of sample powder were measured on a Siemens D5000 Panalytical X'Pert Pro X-ray diffract meter using Cu Kα1 radiation and a fixed power source (40kv and 40ma). Samples were analysed over a range of 4-70° 2θ at a rate of 2.5° per min.

2.2.9.2 Transmission Electron Microscopy

TEM images were obtained with a Philips CM200 transmission electron microscope operating at 200kV. All samples were dispersed in 95% ethanol and loaded on the carbon-coated film for analysis.

2.2.9.3 N2 Adsorption/desorption isotherms

The N2 adsorption/desorption isotherms data was obtained from a Micrometrics Tristar II 3020 particle analyser, samples were dried at 110℃ in vacuum on a Micrometrics Flowprep 060 degasser prior to analysis. The BET equation was applied to determine the surface area.

2.2.9.4 Ultraviolet-Visible light absorption spectra

Uv-Vis spectra were measured using a *Cary 50* UV-Vis spectrometer from *Varian*. Quartz cuvette employed in this part was purchased from Shimadzu Company. The baseline adjustment was conducted prior to each

scan, the blank comparison of samples were their corresponding buffer solutions.

2.2.9.5 Infrared Spectroscopy

IR spectra were obtained from *Nicolet Diamond ATR 5700* spectrometer. Each spectra were co-added by 64scans which over the 4000-525cm^{-1} range with a resolution of 4cm^{-1}. The Al-fiber sample was set as blank sample.

2.3 RESULTS AND DISCUSSION

2.3.1 Characterisation of Supports

2.3.1.1 X-Ray Diffraction

Firstly, XRD technique are utilised to identify the crystallite phase of raw γ-Al_2O_3 nanofibres. As shown in Figure 2.2, the XRD pattern of Al-Fibre exhibits characteristic diffraction peaks match typical γ-Al_2O_3 material at 2θ values of (311), (222), (511) and (440), which indicates the Alumina nanofibres produced in this work are as designed and expected [48].

The further XRD tests were managed on functionalised Alumina nanofibres, the patterns are shown in Figure 2.2 as well. The XRD patterns of silane grafted Alumina nanofibres and GA attached Alumina nanofibres are found to be identical to each other and raw Al-Fibre. The comparison of

three XRD patterns illustrates that silane group and cross-linking agent GA have no impact on the crystal structure of immobilisation support.

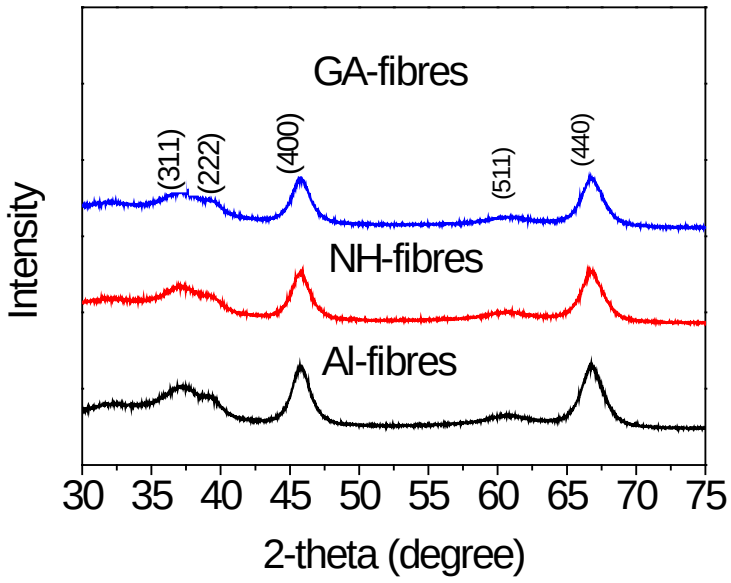

Figure 2.2 Wide-angle XRD patterns of 3 different supports before laccase immobilisation

2.3.1.2 Transmission Electron Microscopy

The image provided by Transmission Electron Microscopy is the direct observation of the morphology of the nanomaterial. Figure 2.3 presents the image of the prepared γ-Al_2O_3 nanofibres, according to the image, the length of Alumina nanofibres is approximately 100-120nm, the width is around 10nm.

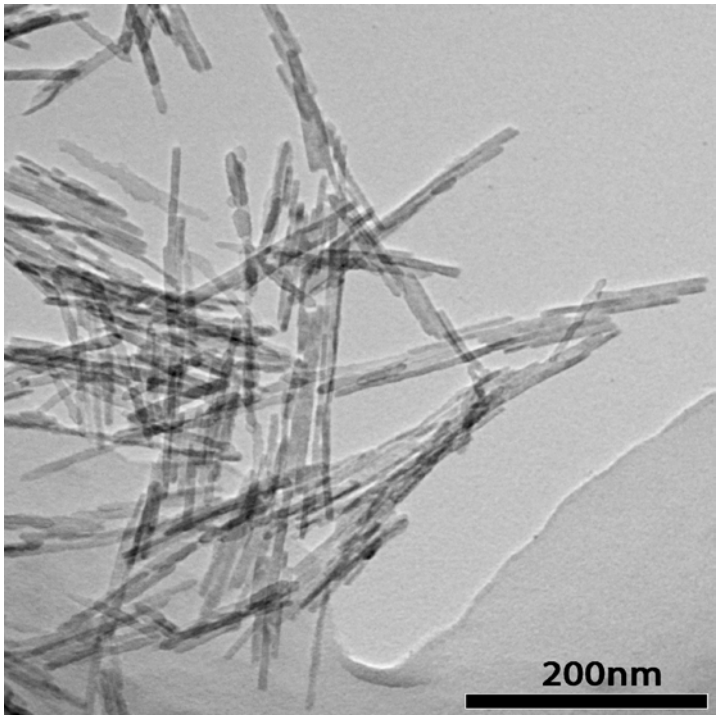

Figure 2.3 TEM image of Alumina nanofibres

2.3.1.3 Surface area of immobilisation support

The surface area data was measured by N2 Adsorption/desorption isotherm techniques and calculated using the BET equation (Table 3.1). The surface area of Al-Fibre supports is found to be 187m^2/g, which is a relative large surface area for this type of Alumina nanofibre structures allowing a great large immobilisation amount possible. On the other hand, the surface area of NH-Fibre and GA-Fibre are respectively 190m^2/g and 180m^2/g. It can be found the surface area of functionalised Alumina nanofibres is close to the original Al-Fibre, which means the type of functional group has very little effect on the morphology of the support surface.

In contrast, the similar surface modification on mesoporous materials, which is widely used in the enzyme immobilisation, normally causes a dramatic reduction in surface area and pore volume.

Sample	Al-Fibre	NH-Fibre	GA-Fibre
Surface area (m^2/g)	187	190	180

Table 2.1 BET data for immobilisation supports of three different kinds.

2.3.1.4 Infrared Spectra

The IR spectra of Al-Fiber, GA-Fiber and the subtracted result are shown in Figure 2.4, the Al-Fibre was presented as blank in order to demonstrate the successful attachment of silane group and GA cross linking agent. In the spectrum of Al-Fiber ranging from 4000cm^{-1} to 600cm^{-1}, no distinguishable peaks can be observed only except the broad signal at 3500cm^{-1} which corresponds to the -OH of alumina crystal surface. On the other hand, in the spectrum of GA-Fiber, the band located at 1068 cm^{-1} corresponds to the stretch of C-O-Si bond, which proves the attachment of silane to Alumina. The conjunction signal of the stretching of -C=N bond is observed around1610cm^{-1}, such band clearly demonstrated the cross-ling of GA group. In addition, the band found at 2919cm^{-1} is corresponding to the –C-H and =C-H stretching which cannot be observed from Al-Fiber sample, it could be a collateral evidence that organic groups were grafted on Al-Fiber [41].

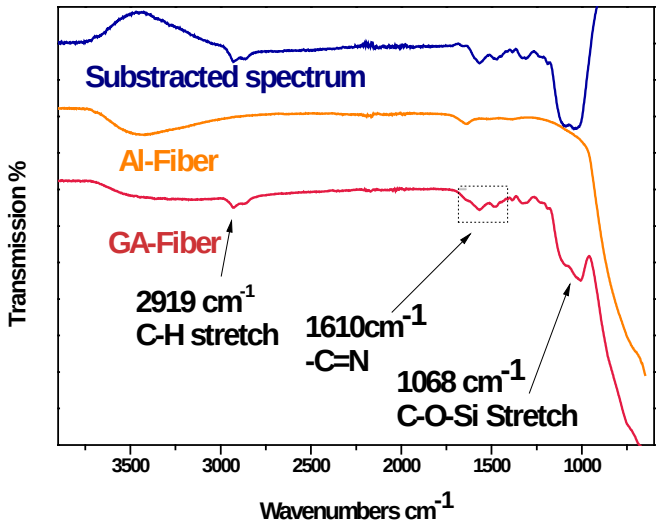

Figure 2.4 IR spectra of the functional group attached Al-Fibre.

2.3.2 Immobilisation of Laccase

The immobilization capacity of supports is shown in Figure 5. The data of laccase immobilization as a function of time is presented in Figure 5a, when laccase concentration is 500ppm and pH value is 7.0, the equilibrium adsorption could be achieved in 90min to all three supports. Due to its large surface area and simple surface morphology, the adsorption duration is incredibly short. Despite the fast adsorption speed, the mount of immobilized laccase is another advantage of functionalized Alumina nanofibres structure. To which, 1 g NH-Fibre can adsorbed 110 mg laccase while 1g GA-Fibre would covalently bond 107 mg laccase, on the other hand, pure 1g Al-Fibre adsorbed only 17mg laccase. The duration that equilibrium adsorption had been achieved for all three supports are parallel, the reason is the morphology of three supports are the same. Although the adsorption speed of Al-Fibre and NH-Fibre are similar, however the difference of adsorption amount between them is enormous where the electrostatic adsorption plays a crucial

role in. Figure 5c presents the zeta potential vs pH value of Al-Fibre, NH-Fibre and Laccase, their measured isoelectric point were 7.78, 9.45 and 2.02 respectively. It is shown that silane grafting has great impact on the electrical property of fibre surface. In the immobilization process where practical pH value was set at 7.0, the laccase protein molecular is strongly negative charged, the measured zeta potential is -32.5mV. On the other hand, NH-Fibre is surrounded by strong positive charge, the measured zeta potential is +27.31mV. The attraction between support and enzyme caused by opposite charges explains the large immobilization amount on NH-Fibre. In contrast, Al-Fibre generates only +5.73 mV of zeta potential under practical condition, such positive charges are so close to neutral that adsorption between support and enzyme is weak and the immobilization amount is dramatically lower then NH-fibre [50][12][51]. In addition, the immobilization capacity of NH-Fibre and GA-Fibre are similar, the reason is that firstly the surface area are same, secondly the amount of –NH end on NH-Fibre are equal to the amount of GA cross-ling agent on GA-Fibre. Even though, the immobilization mechanisms are completely different between the two supports, this will be further discussed in section 3.4.

Figure 5b is presenting an isothermal adsorption curve which illustrates the immobilization capacity as a function of laccase concentration. According to previous results, the period of this experiment was 6 hrs in order to achieve absolute equilibrium adsorption. Firstly, it can be found that the equilibrium adsorption amount of three supports is similar to the Figure3.4a. 1 g raw Al-Fibre adsorbed only 14mg laccase at pH value 7.0. On the other hand, NH-Fibre and GA-Fibre have relatively large immobilizing amount of laccase at the same pH value, 1 g NH-Fibre is capable of adsorbing 110mg laccase and saturated adsorption of 1g GA-Fibre is

105mg laccase. Besides, the maximum adsorption could be achieved where the environmental laccase concentration is higher than 200ppm, the maximum adsorption amount remains the same when the laccase concentration increasing higher even to 800ppm, that is also the reason that 1000ppm laccase was applied in the experiment of laccase immobilization as a function of time.

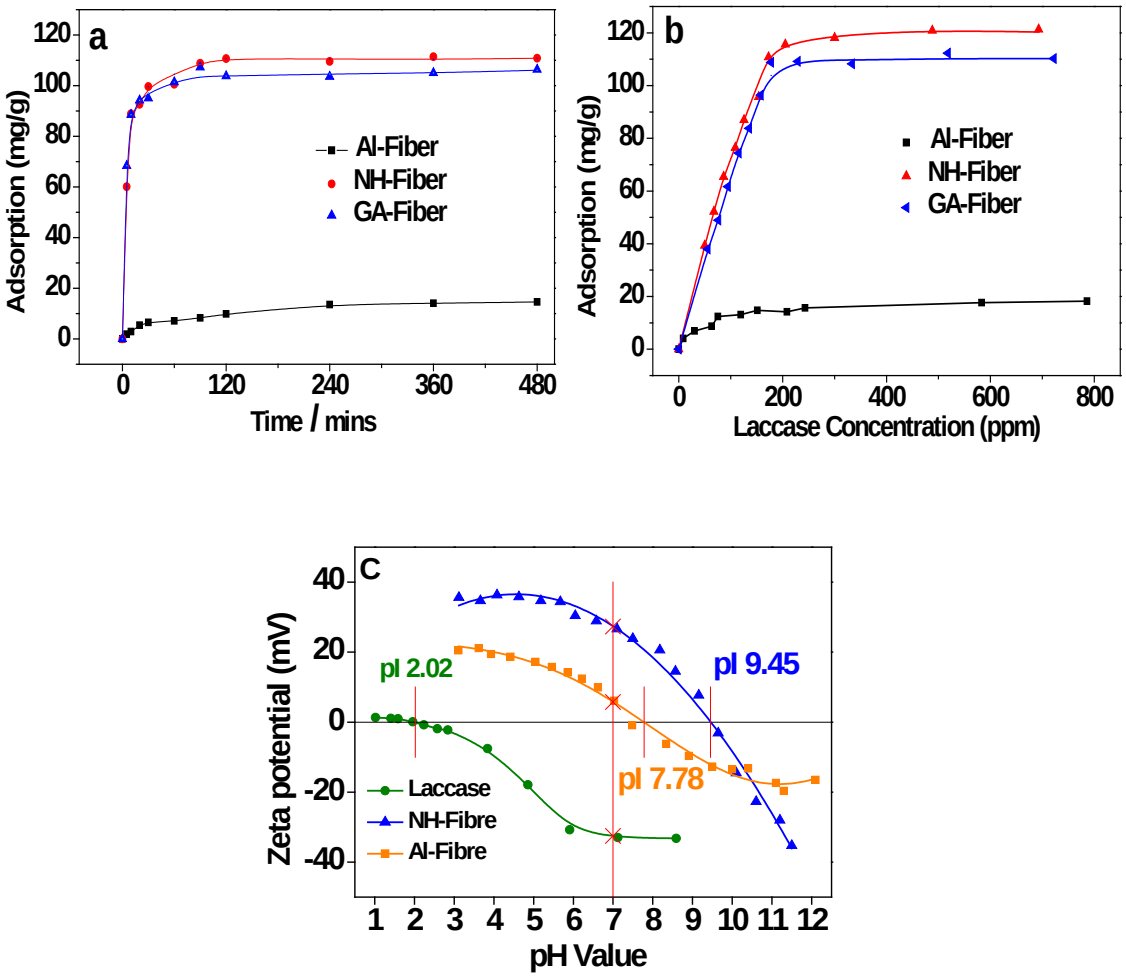

Figure 2.5 (a) Immobilised amounts of laccase on the supports as a function of time. (b) Immobilised amounts of laccase on the supports as a function of laccase concentration. (c) Zeta potential vs pH value of Laccase and NH-fibre.

2.3.3 Activity of the Immobilised Laccase

The activity of laccase was defined as the ability of transferring ABTS to $ABTS^+$. As previously stated, 1 unit of laccase activity corresponds to the amount of laccase which convert 1μmol ABTS to $ABTS^+$ per minute.

No matter the enzyme is physically adsorbed or covalently bonded on support, the immobilisation process would have impact on the enzymatic activity because of the change of surface charge and spatial structure on enzyme molecular, in most cases, the impact is negative. As a consequence, to what extent the enzymatic activity can be recovered after immobilisation process becomes the great concern of immobilisation technique. In this work, the activity test comparison between free laccase and immobilised laccase was conducted at pH value 4.5 and temperature 20 as recommended by chemical supplier. The results are shown in Figure 2.5.5.

It can be found that 87.3% of the activity was retained on laccase supported by NH-Fibre. In comparison, the laccase on GA-Fibre retained 76.1% of the activity which is slightly lower than NH-Fibre due to the structure impact causing by covalent bond. In sum up, the activity recovery ratio of both the two immobilisation processes are remarkably high.

Enzymes	Activity of laccase (U/mg)	Recovery yield of laccase (%)
Free laccase	10.327	100
Laccase-NH-Fibre	9.012	87.3
Laccase-GA-Fibre	7.862	76.1

Table 2.2 Activity recovery ratio of immobilised laccase

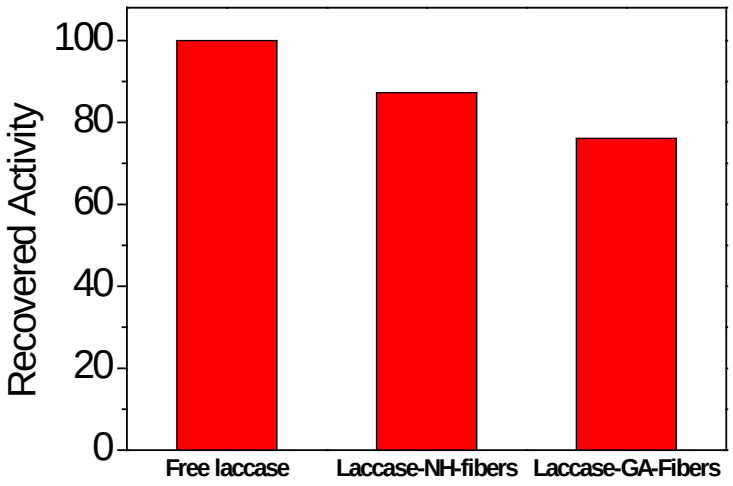

Figure 2.6 Resistance of pH value and temperature comparison between Free Laccase and Immobilised Laccase.

2.3.4 Resistance to pH value and temperature

As a biocatalyst, the activity of enzyme only exists in a relatively small range of pH value and temperature, thus the resistance to pH value and temperature change is of significant importance to the natural property of enzyme. Due to the similar reason on the enzymatic activity, the immobilisation process has impact on this property. However, on the contrary the immobilisation process normally increases the resistance ability of enzyme to the environment, because the immobilisation of enzyme is also the reinforcement of the spatial structure.

Figure 2.7 shows the activity of free and immobilised laccase at different pH values from 3.0 to 7.0. In order to display comparison, the activity ratio was given rather than actual activity unit, the pH value of 100% activity was set on the basis of experiment results. It can be found that the enzyme laccase prefers to the low pH

value environment, the activity was completely lost when pH value reaches 7.0 and the optimised pH value for both free laccase and immobilised laccase is 4.0. The result also demonstrated that immobilisation process enhanced the ability of laccase to resist the pH value change, the immobilised laccase exhibits higher activity ratio in the pH range from 3.0 to 6.0, however the activity of immobilised laccase was completely lost at pH 7.0 as same as the free laccase.

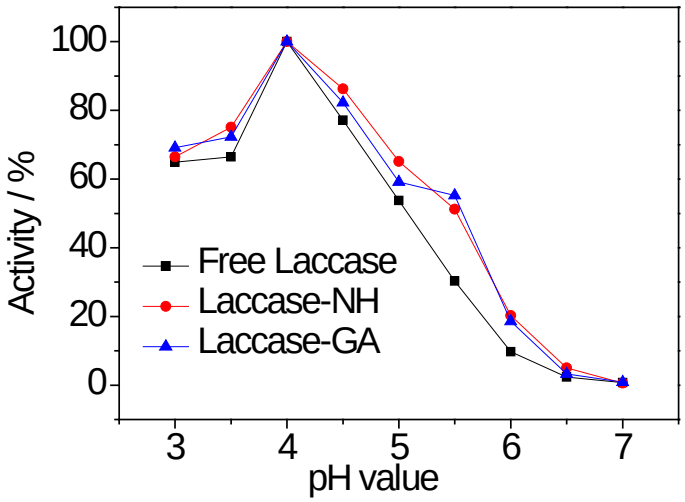

Figure 2.7 Activity of the free and immobilised laccase at different pH values.

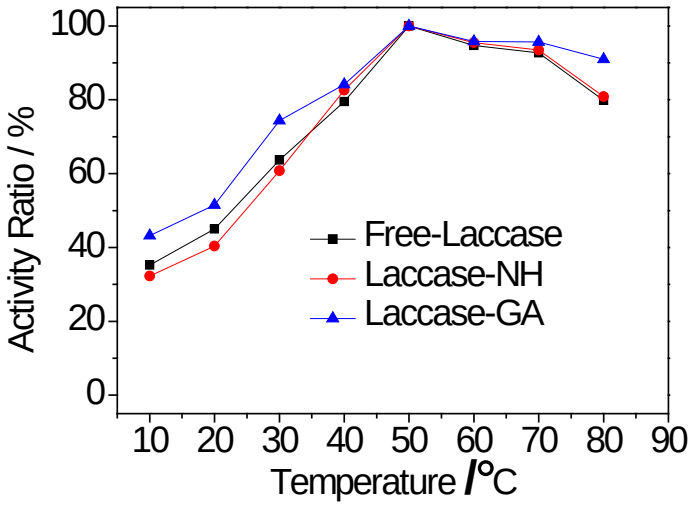

Figure 2.8 Activity of the free and immobilised laccase at different temperature.

Figure 2.8 displays the effect of temperature on the activity of the free and immobilised laccase, the results are shown as the ratio to the maximum activity as well. In normal chemical reactions, the reaction rate usually increases as the temperature is raised. However, in enzymatic reaction, the temperature increasing could cause denaturation of enzyme molecular by destroying the quaternary structure and results in the dramatic decreasing of reaction rate. According to the experimental data, laccase adapt to relatively high temperature, it exhibits maximum activity at 50℃, nearly 75% activity remains when heated up to 80℃. On the other hand, the activity dropped rapidly when temperature reduced below 50℃, only 30% of activity was retained at 10℃ for free laccase and 42% for laccase immobilised on GA-Fibre. Comparing with free laccase and physical adsorbed laccase, the covalently bonded laccase exhibits higher activity ratio in the whole temperature range from 10℃ to 80℃, which means immobilisation process can improve the thermal stability of laccase. That is because covalent bonding stabilised laccase on molecular level and reduced the damage to spatial structure.

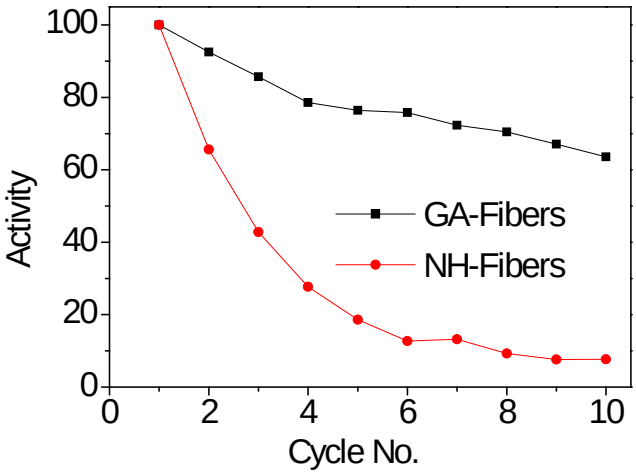

Figure 2.9 Reusability of laccase on NH-Fibre and GA-Fibre.

2.3.5 Reusability

To determine the reusability and investigate the mechanism of the immobilisation of laccase on NH-Fibre and GA-Fibre, the immobilised laccase was introduced into a continuous cycle reaction. The results of 10 cycles of constant reaction were shown in Figure 2.9, it can be found that 63% activity of immobilised laccase was retained on GA-Fibre after the cycles reaction. In contrast, activity of laccase on NH-Fibre reduced rapidly, only 12% activity remained on NH-Fibre after 5 cycles and it ends at 7% after 10 cycles. The reusability performance of immobilised laccase not only demonstrated that laccase immobilised on GA-Fibre can be applied in a relatively long term application, it also indicates that there is no strong bonding force between laccase and NH-Fibre support as it can be rinsed from support. In the contrast, the laccase immobilised on GA-Fibre is much more stable and proven to be covalently bonded.

2.4 CONCLUSION

The precursor of γ-Alumina nanofibres was synthesized by the hydrothermal reaction of $Al(NO_3)_3 \cdot 9H_2O$ and TEAOH at 170℃, the reaction period was 72 hours and the pH value was adjusted to precise 5.0 to obtain boehmite nanofibres. Boehmite nanofibres were transferred to γ-Alumina when calcining at 550℃, then the Alumina nanofibres of average 80-120nm length and 10nm width was prepared.

Alumina nanofibres was functionalised with group APTES and cross linking agent Glutaraldehyde for enzyme immobilisation. The attachment of functional group and cross linking agent was determined by IR spectra.

Laccase from *Trametes versicolour* was covalently immobilised on fully functionalised Alumina nanofibres. The raw Alumina nanofibres and silane only functionalised Alumina nanofibres was applied in the same immobilisation process through physical adsorption method, these two supports were set as comparison.

The immobilisation capacity and of different supports was tested as long as the influencing factor for the equilibration adsorption. A relatively large amount of laccase has been immobilised in this experiment and the immobilised laccase retained its activity to a great extent.

The thermal and pH stabilities of immobilised laccase was tested and proven to be improved as compared to the free laccase. In addition, the immobilised laccase was introduced into a cycle reaction test, during which, the covalent bonded laccase exhibited much better reusability compare to physical adsorbed laccase.

Chapter 3: Modified Alumina Nanofibres Coating on Porous Alumina Supports for Protein Separation

3.1 INTRODUCTION

Large-scale purification/separation of bio-substances is a key technology required for rapid production of biological substances in bioengineering. Among which, highly efficient protein separation is an essential process of great importance in molecular biology research for the isolation, purification and recovery of proteins and enzyme in pharmaceutical, food and medical industries [52] [53] [54] [55]. In most cases, protein separation is not only a technical challenging but also a critical limiting factor in large-scale biological production. Conventional separation techniques involve labor-intensive and time consuming processes, such as precipitation, filtration, centrifugation, crystallization, resolution-focused affinity chromatography and electrophoresis purification [56] [57] [58]. For example, ammonium sulphate was commonly applied in the bulk protein purification, the surface charge of proteins is being changed and causes protein denaturation, and consequently proteins are isolated from solvent by precipitation and filtration processes. However, the roughness of such technique and the damage caused on protein molecular limits its further applications in fine bio-production. For the analytical protein separation, chromatography is the mostly applied technique, which includes gel permeation

chromatography based on the size exclusion strategy, ion exchange and hydrophobicity chromatography based on the surface interaction of protein and other specific chromatography techniques [59][60]. Although effectiveness of chromatography technique is widely accepted, it is still restricted by its limited scale and efficiency due to the low flow rate and expensive chromatographic support.

With the progress in separation technology and advanced materials, membrane filtration has attracted much attention due to the potential for improvements in flow rate, energy savings, operation costs, and environmental impacts. As a consequence, the ultra-filtration membrane technology was introduced into this field dependent on size exclusive, surface charges and interactions [61]. These membranes were fabricated by two major materials which are polymeric and ceramic materials [62] [55]. Due to low cost and ease of fabrication, bulk of research papers focus on electrospun fibers polymer ultra filtration membranes which have pore sizes ranging from 1 to 100nm [63] [64] [65] [66] [67]. For example, cellulose acetate fibre, which was utilised in the very first polymer ultra-filtration membrane, is a wildly applied material with various modifications [68]. Sivakumar M. and Mohan R.D fabricated the cellulose acetate ultra-filtration membrane and it was functionalised by polysulfone, such functionalised membrane was managed to reject 90% of BSA protein with molecular weight of 69 kDa and 60% of Trypsin of molecular weight 20kDa, the corresponding permeate flux were 74.5 $L \cdot h^{-1} \cdot M^{-2}$ and 83.7 $L \cdot h^{-1} \cdot M^{-2}$ under high pressure of 345KPa [69]. In addition, many other functional groups and materials have been reported to be incorporated with cellulose acetate to achieve performance enhancement, such as amphiphilic copolymer Pluronic F127 which improved the water flux to 100 $L \cdot h^{-1} \cdot M^{-2}$ at lower pressure of 150KPa [70][71]. Inorganic materials such as Silica particles had been applied to modify the cellulose acetate ultra-filtration membranes as well,

the results indicate that the rejection of BSA reaches 95% and decreases with the increase of Silica ratio, however only 46.76 $L \cdot h^{-1} \cdot M^{-2}$ of water flux was observed under pressure 345KPa [72]. Other than cellulose acetate and polysulfone materials, poly vinyl membrane has attracted significant attention as well. For instance, Poly vinylidene fluoride membranes had been blend with amphiphilic poly methacrylates and poly ethylene oxide in order to resistant proteins [73]. Moreover, Yu and Lee introduced Au nanotubules into the pores of polycarbonate template membranes for the size based protein separation and illustrated the relation between Au nanotubules diameter and the selectivity of protein separation [74]. Through all the attempts that utilising polymer ultra-filtration membrane in the purpose of protein separation and filtration, it can be found that in most cases the polymer membranes were succeeded in rejecting major parts of the target protein from solvent where the protein molecular weight decreases to 20KDa. The water flux of polymer membranes are mostly no larger than 100 $L \cdot h^{-1} \cdot M^{-2}$ at high pressure of 300KPa even though they are better than chromatography method. It still significantly restricts the performance of polymer ultra-filtration membrane in large scale application. Meanwhile, the researches of polymer membranes indicate that the surface hydrophobicity is able to make great improvement on the protein rejection.

Even through, the selectivity of polymer membrane achieved a fairly high ratio, the low permeation flux urged researchers to develop new membrane materials, especially for proteins with diameters of 1-10nm and sensitive to minor differences in protein properties. Therefore, ceramic materials such as zirconium, titanium and aluminium oxide were extensively studied for the separation of protein due to the

outstanding mechanical strength and thermal stability [75]. Additionally, many innovative techniques have been developed to enhance the efficiency of membrane processes. Ceramic nanoparticle materials had attracted the first attention, wide range of nano particles of various types were applied such as TiO_2, ZnO, Al_2O_3 and Silica [76]. Researchers firstly attempted to combine the organic membrane and ceramic nanoparticle [77][78][79][80], they studied the impact of nanoparticles on morphology and performance of the organic membranes, the decreased water flux caused by decreased porosity had been observed as well as the enhanced protein resistance. In order to obtain higher penetrant rate, researchers then focused on the pure ceramic membrane which are typically formed by a substrate layer and a thin separation layer [81]. Rabiller-Baudry fabricated an ultra-filtration system which consisted by Alumina base and the separation layer composed by zirconium particles of diameter 1μm [82]. They tested the ultra filtration performance of the membrane to both single protein solutions (lysozyme and lactoferrin) and mixed protein solution, it was found that the membranes modified with pyrophosphate or ethylenediamine groups exhibits higher selectivity than original membranes, they suggested that the electrostatic interaction between modified membranes and proteins has great contribution to the membrane performance. On the other hand, some researchers designed the separation layer in mesh structure using ceramic nanofibre material to increase permeation flux while maintaining the high selectivity. According to Ke, in order to improve the selectivity of membranes consisted of particles which is defined as conventional ceramic membrane, the particles size should be correspondingly reduced in order to reduce the pore sizes, such reduction causes serious flux loss [83]. Besides, the formation of particles in conventional membrane inevitable creates a great amount of dead-end pores which decreases the porosity of membranes. Due to these inherent

disadvantages, the conventional ceramic membranes are unable to possess the high flux and selectivity at the same time, consequently ceramic nanofibres is attracting increasing interest [84]. The structure of nanofibres membrane is basically mesh-like which is known as the most efficient in filtration system, the porosity of the nanofibres layer can be over 70% in contrast to the below 36% of the conventional membrane [47]. In the fabrication of nanofibres membranes, researcher tend to prepared bi-layer system, the top layer was separation layer made of nanofibres for the filtration purpose and the bottom layer was support layer made of porous ceramic material for mechanic support and high flux. For example, Ke managed to coat one layer of Titanate nanofibres on the top of porous α-Alumina and glass support and then one layer of Alumina nanofibres above, the separation performance of prepared membrane was tested by standard latex sphere where 97.3% of 108nm spheres were rejected, while the water flux of the membrane reaches 4000 $L \cdot h^{-1} \cdot M^{-2}$. Furthermore, Ke reported another novel method for nanofibres membrane fabrication, the aluminium hydroxide, which is the precursor sol-gel of Alumina nanofibres, was filled into the pores of the α-Alumina support and *in-situ* transferred to Alumina nanofibres, such membranes was applied in the separation of protein and DNA molecular and achieved the rejection of 93% of 12nm size protein at a flux of 95.4 $L \cdot h^{-1} \cdot M^{-2}$, in the contrast, the flux of polymer membrane which has similar achievement was reported to be less than 60 $L \cdot h^{-1} \cdot M^{-2}$ [47] [85] [82]. In addition, not only Alumina nanofibres, Titanate nanofibres has been reported to be utilised in ultra-filtration membranes, Qiu sintered Titanate nanofibres on the surface of α-Alumina tubes in the presence of polyvingl alcohol, the fabricated membrane exhibits extraordinary water flux of 4000 $L \cdot h^{-1} \cdot M^{-2}$ while the molecular weight cut-off (MWCO) is 32KDa [84]. It can be found that the ceramic nanofibres membrane

achieved a new grade of water flux while maintaining the same separation efficiency, yet there are still enormous of nanofibres of different materials and types can be applied in the fabrication of ceramic ultra-filtration membrane. Moreover, the ceramic membranes could be functionalised following the strategy of polymer membranes as described above to enhance the performance.

In this study, synthesis condition of Alumina nanofibres was optimized and a series of characterisations was conducted. Then the prepared Alumina nanofibres were dip coated on the porous α-Alumina disc support to form bi-layer membranes for protein separation. To combine the sieving effects and surface properties of the fiber membranes, the membranes were functionalised with silane group to modify the membrane surface to hydrophobicity, such modification improved selectivity while retained a high permeating flux. Gel permeation chromatography (GPC) is used to indirectly determine the pore size, the surface contacting angle analysis was applied for measuring the wetting property. The water flux of the membranes of each step was measured to illustrate the penetration property, the MWCO of the membranes was determined by standard dextran solution and the protein separation tests were conducted using BSA, cellulase and Trypsin to demonstrate the performance of resultant membranes.

3.2 EXPERIMENTAL

3.2.1 Materials

Unless otherwise stated, all the chemicals were commercially purchased from suppliers and used without any further purification. Albumin from bovine serum powder (BSA), Cellulase from *Trichoderma viride,* Trypsin from bovine pancreas,

(3-aminopropyl) triethoxysilane (APTES) and Polyglycol ether surfactants (T15S-7) were purchased from Sigma Aldrich. Dextran from *Leuconotoc mesenteroides* of M.W. 10,000, 40,000, 70,000 and 500,000 were purchased from Sigma Aldrich. $NaAlO_2$ and Acetic acid are of analytical grade. Phosphate buffer solution (PBS) was prepared by NaH_2PO_4, Na_2HPO_4 and KH_2PO_4. The Membrane α-Alumina disc supports were supplied by Membrane Science and Technology Research Centre of Nanjing University of Technology, the disc supports are of 30mm in diameter and 2mm in thickness and have a mean pore size of 0.8 μm. All other chemicals used in the experiment were of analytical grade.

3.2.2 Fabrication of surface functionalised Alumina Nanofibres membrane

3.2.2.1 Synthesis of Boehmite Nanofibres

The boehmite nanofibres was prepared by the hydrothermal reaction involves $NaAlO_2$ and acetic acid in the presence of surfactant. Firstly, 9.4g of $NaAlO_2$ was dissolved in 25 ml of deionised water, and then the above solution was dropwise added into 50ml of 5mol/L acetic acid solution under vigorously stirring. A white precipitate was obtained and recovered by centrifugation and then washed with deionised water for 4 times to remove Na^+. 2g of T15S-7 surfactant was mixed into the aluminium hydrate cake under vigorously stirring, the pH value of the mixture was precisely adjusted to 5.0 using ammonia. After 1 hour of stirring, the mixture was transferred into closed autoclave and kept in oven. The

obtained wet cake was washed with deionised water 3 times and ethanol once.

In order to optimise the reaction condition, the synthesis procedure was conducted at different reaction temperature of 130℃ and 180℃. The reaction period was studied as well and set to 12hours, 24hours, 48hours and 72hours in this experiment.

The prepared boehmite nanofibres were calcined at 550℃ for a period of 5 hours to convert to γ-Al_2O_3 nanofibres for further property test.

3.2.2.2 Alumina Nanofibres coating on Support Membrane

The prepared boehmite nanofibres was coated on the surface of Alumina disc support as shown in Figure3.1, the raw disc was labelled as Blank-Membrane. The nanofibres were loaded by dip coating where 0.05MPa vacuum was added beneath the disc. The excess precipitate on the top surface was removed simply by scraping and flushing [24]. The boehmite coated disc was labelled as Bo-Membrane.

The boehmite nanofibres coated support was then placed in Muffle furnace for subsequent calcination at 500℃ for a period of 5 hours. During which, the boehmite nanofibres layer was converted to γ-Al_2O_3 nanofibres and firmly attached on the surface of support.

The above procedure was repeated 3 times on each disc support to ensure the complete cove. The prepare disc support was labelled as Al-Membrane.

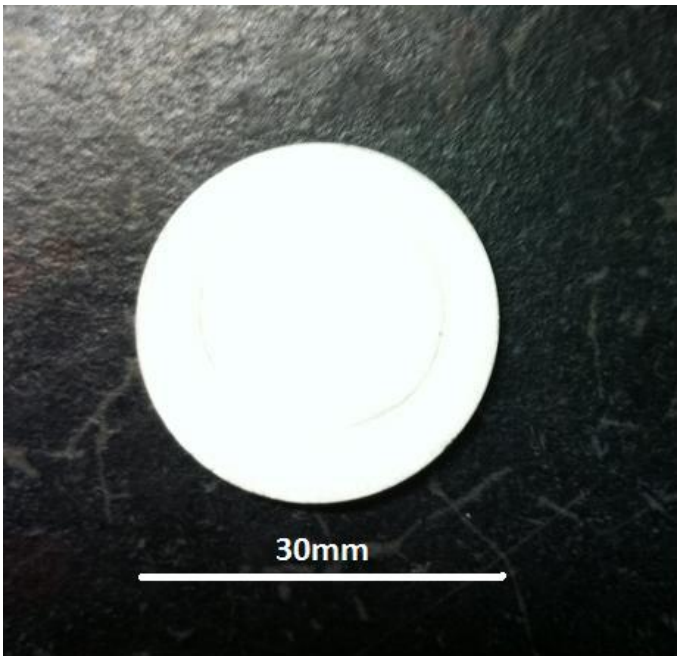

Figure 3.1 Alumina disc support.

3.2.2.3 APTES grafting on Alumina Nanofibres coated Membrane

The APTES group was introduced to the prepared Al-Membrane to for a hydrophobic modification. The experiment procedure is as follow: Prepared Al-Membrane was immersed and suspended in the anhydrous toluene, to the toluene 0.9g of APTES liquid was added. The system was heated to 110℃ in oil bath and kept for 48hours under stirring. The recovered disc was rinsed with pure ethanol and dried in air at 60℃. The final obtained disc was labelled as NH-Membrane.

The ABTES grafting was also carried out on the γ-Al_2O_3 nanofibres which mentioned in section 3.2.1, the experiment procedure refers to section 2.2.3. The NH-Fibre was prepared for characterisation as well as γ-Al_2O_3 nanofibres.

3.2.3 Performance of Ultra-filtration Membrane

3.2.3.1 Permeability Efficiency

The permeability efficiency was determined by water flux and compared between Membranes of 4 stages. The peristaltic pump was applied as pressure source. In this experiment, due to the function way of our peristaltic pump, the flow rate was set as still and the pressure was measured and recorded.

The deionised water was applied as penetrant and the diameter of effect area of loaded membrane is 20mm.

3.2.3.2 Dextran Retention Test

The standard dextran solution was employed in the retention test of membrane for the MWCO test. Dextran from *Leuconotoc mesenteroides* of 4 different M.W. were selected which are 10,000, 40,000, 70,000 and 500,000. The experiment system was the same to permeability efficiency section. The standard dextran solution of 1000ppm was employed as penetrant, the pressure was stabilised at 145 psi by adjusting the flow rate. The concentration of penetrated dextran solution was measured by gel permeation chromatography (GPC) technology.

The MWCO was determined by comparing the concentration of penetrated dextran solution to the original dextran solution.

3.2.3.3 Protein Separation Efficiency

In this section, the experiment system was the same to the previous only except the penetrant was changed to protein solution. BSA, Cellulase and Trypsin were employed in the protein separation test because of the step-down molecular weight which are 66K Da, 45K Da and 23.8K Da respectively. The protein concentration was determined by Uv-Vis spectroscopy and a standard curve was created prior to sample analysis. The separation efficiency was determined by comparing the concentration of penetrated protein solution to penetrant solution. The effect of penetrant concentration on the separation efficiency was studied on the range of 0-1000ppm.

3.2.4 Characterisation Techniques and Instruments

3.2.4.1 BET N_2 adsorption

The N_2 adsorption/desorption isotherms data was obtained from a Micrometrics Tristar II 3020 particle analyser, samples were dried at 110℃ in vacuum on a Micrometrics Flowprep 060 degasser prior to analysis. The BET equation was applied to determine the surface area.

The Boehmite nanofibres, γ-Al_2O_3 nanofibres and NH-Fibre were involved in the N_2 adsorption test for the comparison.

3.2.4.2 Transmission Electron Microscopy

TEM images were obtained with a Philips CM200 transmission electron microscope operating at 200kV. All samples were dispersed in 95% ethanol and loaded on the carbon-coated film for analysis.

3.2.4.3 Field Emission Scanning Electron Microscopy

The Field Emission Scanning Electron Microscopy (FESEM) was utilised to directly observe the morphology of the membrane surface. The images were obtained with a JEOL JSM 7001f instrument operating at 10kV. All samples were coated with gold to improve the conductivity and deposited on the carbon-coated film prior to analysis.

3.2.4.4 X-ray Diffraction

The wide-angle X-ray diffraction (WAXRD) patterns of sample powders were measured on a Philips Panalytical X'Pert Pro X-ray diffract meter using Cu Kα1 radiation and a fixed power source (40kV and 40mA). Samples were analysed over a range of 4-70° 2θ at a rate of 2.5° per min.

The X-ray Diffraction analysis was conducted directly on the disc samples with specified sample carrier, as a consequence, the X-ray Diffraction pattern presents the crystal information of disc surface.

3.2.4.5 Gel permeation chromatography

The GPC spectra were obtained from Waters HPLC system using RI detector and running 0.2M sodium dihydrogen phosphate pH7.0

solvent at 1 ml/min. The column was a 2*7.8*300nm water ultra-hydro gel linear column. A standard curve of dextran solution was created prior to sample analysis.

3.2.4.6 Contact Angle Analyser

The surface contact angle of analysed by a Nanotech FTA200 Contact Angle Analyser. All disc samples were dried in air at 60℃ over night prior to the test.

3.2.4.7 Pore Size Distribution Test

The pore size distribution of the membranes was indirectly measured by using the liquid to liquid displacement method. Firstly, isopropanol was mixed with deionised water in 1:1 volume ratio, after stratification the mixture was separated to isopropanol rich phase (oil phase) and water rich phase (water phase). Membranes were immersed in oil phase in vacuum overnight to fill pores with liquid, such filled membrane was named wet membrane. The wet membranes were set in pumping device in order to displace the oil phase liquid with water phase liquid. By monitoring the pressure and the flow rate, the corresponding pore radius opened at a given applied pressure can be calculated using the Laplcase equation:

$$\Delta P = \frac{2\delta cos\theta}{r}$$

Where ΔP is the applied pressure in Mpa, r is the equivalent proe radius in meter, δ is the interfacial tension between water and

isopropanol, θ is the contact angle which was set as approximate value 0 degree in this case.

Assuming that the pores are cylindrical and by using the Hagen-Poiseuille equation, the number of pores that opened can be correlated by:

$$Q_i = \sum_{k=1}^{i} \frac{n_k \pi r_k^4 P_i}{8\eta l}$$

Where Q_i is the volumetric flow, r_k is the pore radius, P*i* is the pressure, η is the dynamic viscosity of the water and *l* is the pore length which is set as membrane thickness [86].

3.2.4.8 Thermo-gravimetric Analysis

Thermo-gravimetric analysis of boehmite nanofibres was carried out in a TA Instruments incorporated series Q500 high-resolution thermo-gravimetric analyser in a flowing nitrogen atmosphere. The sample was placed in an open platinum plate and heated up to 1000℃ at the rate of 10℃ per min.

3.2.4.9 FTIR spectroscopy

*FT*IR spectra were obtained from *Nicolet Diamond ATR 5700* spectrometer. Each spectra were co-added by 64scans which over the 4000-650cm^{-1} range with a resolution of 4cm^{-1}.

3.3 RESULTS AND DISCUSSION

3.3.1 Effect of Temperature on the Synthesis of Boehmite Nanofibres

To investigate the effect of reaction temperature on the boehmite nanofibres growth, the hydrothermal synthesis was conducted at 130℃ and 180℃, the reaction period was 24 hours. The Figure 3.2 displays the TEM images of these prepared boehmite nanofibres where Figure3.2 (a) refers to the boehmite nanofibres synthesized at 130℃ and Figure3.2 (b) refers to 180℃.

It can be found that the boehmite nanofibres were better shaped at lower temperature, the average length of boehmite nanofibres was 80-140nm. In the contrast, the boehmite nanofibres synthesized at 180℃ was much shorter and length was ranging from 40nm-90nm. However, the width of these two boehmite nanofibres samples are the same, the average width is 7-9nm. The result indicates that the lower synthesis temperature 130℃ is beneficial to the growth of boehmite nanofibres rather than higher temperature 180℃. Therefore, the synthesis temperature130℃ was determined as optimised reaction condition.

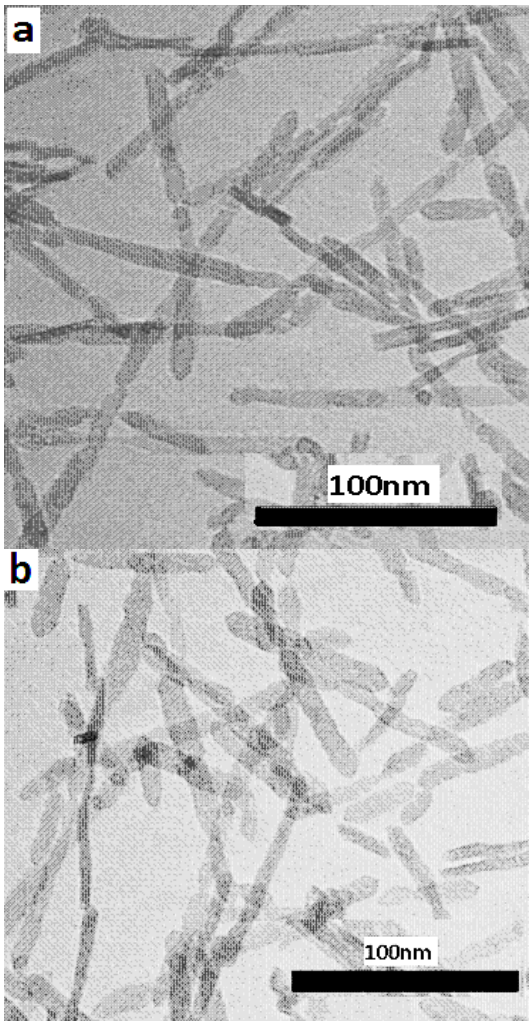

Figure 3.2 TEM images of Boehmite nanofibres as effect of reaction temperature. (a) Boehmite nanofibres synthesized at 130℃. (b) Boehmite nanofibres synthesized at 180℃.

3.3.2 Effect of Reaction Time on the Synthesis of Boehmite Nanofibres

The boehmite nanofibres synthesis on effect of reaction time was studied where the reaction temperature was set at 130℃ based on the last section. The images shown in Figure 3.3 are TEM images of different synthesis period. Figure 3.3 (a) is the images of boehmite synthesized in 12 hours, according to this TEM image, the boehmite nanostructure had been formed within 12 hours yet not complete, the edge of each individual nanofibres is not clear and many fragments can be observed. Figure 3.3 (b), (c) and (d) are the images of

boehmite synthesized in 24 hours, 48hours and 72 hours respectively. In can be found that the boehmite nanofibres structure was kept growing with the synthesis time increasing. After 48 hours of growing, the boehmite nanofibres appeared to be complete and fully distinguishable. However, the boehmite nanofibres synthesis in 72 hours has been found no better than those in 48 hours. Thus, the reaction period of 48 hours has been selected when taking time efficiency into consideration.

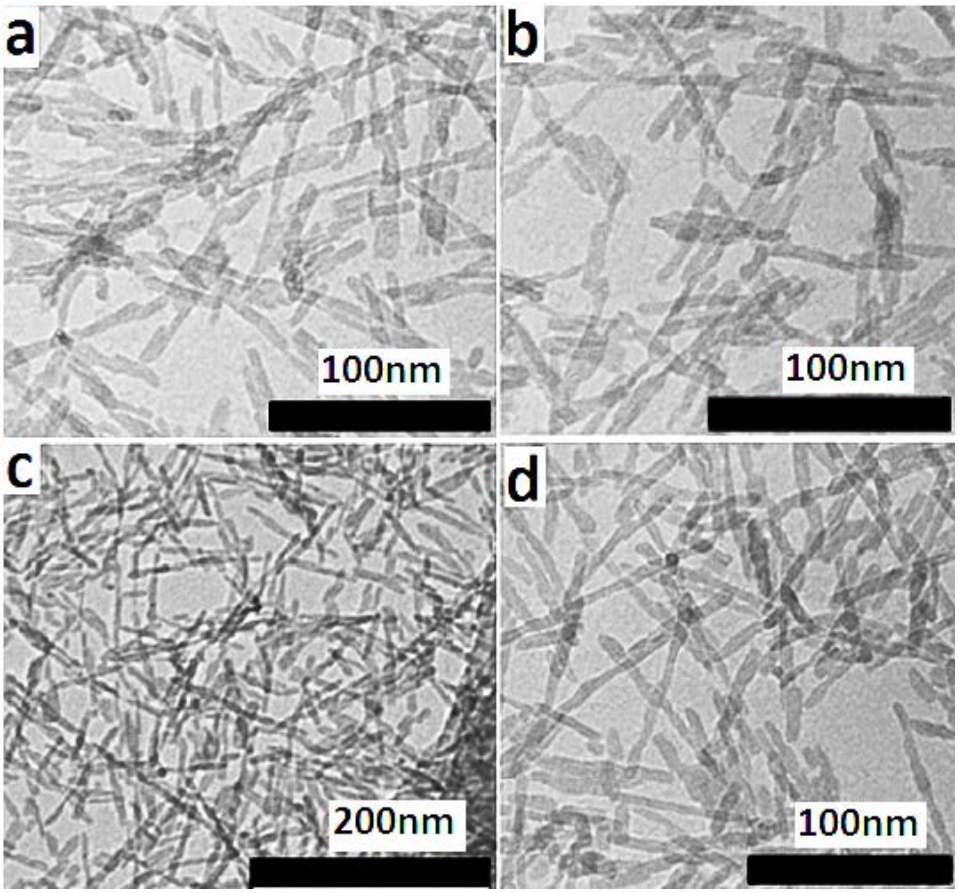

Figure 3.3 TEM images of Boehmite on effect of reaction time. (a) Boehmite nanofibres synthesized in 12 hours. (b) Boehmite nanofibres synthesized in 24 hours. (c) Boehmite nanofibres synthesized in 48 hours. (d) Boehmite nanofibres synthesized in 72 hours.

3.3.3 Characterisation of Boehmite Nanofibres and Ultra-filtration Membrane

3.3.3.1 Surface area

The BET results are displayed in Figure 3.4. The surface area of Boehmite nanofibres is 147m^2/g, it deceases with the increase of synthesis period, the Boehmite nanofibres of 72 hours exhibits surface area of 125 m^2/g. The surface area result of Al-Fibre shows the same trend where the surface area of 12 hours Al-Fibre is 260m^2/g and 72 hours Al-Fibre is 200m^2/g, such trend demonstrated the increase of crystal size which described in TEM result. In addition, it can be found that Alumina nanofibres exhibits the surface area very similar to APTES functionalised Alumina nanofibres, the difference between them are less than 10 m^2/g, the similarity indicates that the surface morphology remains the same after APTES grafting. However, the surface area of boehmite nanofibres, the precursor of Alumina nanofibres, is lower than calcined Alumina nanofibres and functionalised Alumina nanofibres, the reduction is dramatic considering their similar morphology. The explanation is the residual surfactant on boehmite nanofibres has negative impact on the N^2 adsorption process and it can only be burned out in calcine but cannot be simply washed by water.

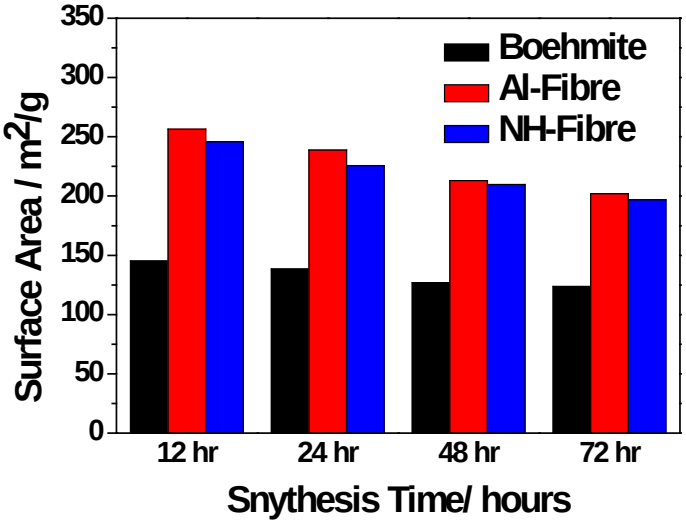

Figure 3.4 N^2 adsorption result of three nanofibres of different reaction time.

3.3.3.2 Thermo-gravimetric Analysis

The Figure 3.5 (a) is the TG curve of boehmite nanofibres and Figure 3.5 (b) is the DTG curve which indicates the change of boehmite nanofibres mass loss rate. Firstly, the dehydration contributes to the weight loss below 100℃, the weight loss in this stage is not significant due to the pre-dry of sample. By comparing the TG curves of boehmite fibre from different synthesis period, the similar results can be observed that the main weight loss from 90% to 60% occurs between 300 ℃ and 450℃. However, the DTG curves, on the other hand, verified two separated mass loss process in this stage. When temperature increased to around 350℃, the adherent surfactant on boehmite fibre was burned out, it causes a sharp peak on DTG curve of

each boehmite sample. The great amount of adherent surfactant is the reason why boehmite nanofibres exhibit low N_2 adsorption. The other peak can be found around 450 ℃ in DTH curves which suggesting the boehmite fibre was converted to γ-Alumina fibre. It can be found that this peak was broad where the boehmite nanofibres synthesis is of 12 hours period, with the synthesis time increasing, this peak became narrow and distinguishable. The boehmite nanofibres of 72 hours synthesis period exhibits the best shaped peak which illustrate that the crystal structure of boehmite nanofibres is complete after 72 hours growth.

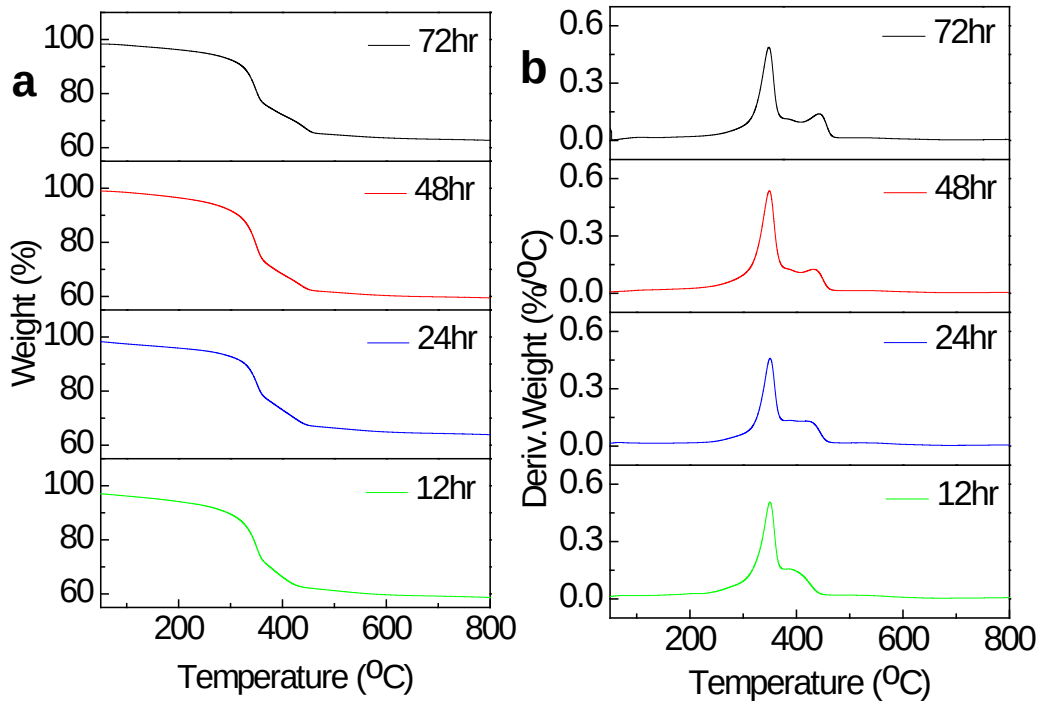

Figure 3.5 (a) Thermo-gravimetry of Boehmite nanofibres (TG), (b) Derivative Thermo-gravimetry (DTG) of Boehmite nanofibres.

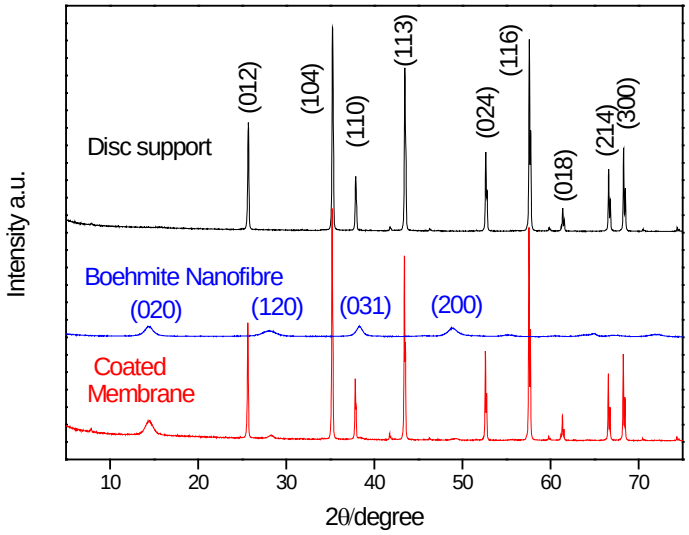

Figure 3.6 XRD pattern of Boehmite nanofibres, Original disc support and Boehmite nanofibres coated support.

3.3.3.3 X-ray Diffraction

Figure 3.8 shows the X-ray Diffraction pattern of Original Disc Support, Boehmite Nanofibres and Boehmite Nanofibres coated Membrane. From these patterns, the Boehmite material exhibits the characteristic peaks differ from Original Disc Support. However, these characteristic peaks were possessed by Boehmite Nanofibres (JCPDS PDF No.21-1307) coated membrane, therefore it can be proved that Boehmite nanofibres had been successfully coated on the surface of Disc Support.

3.3.3.4 Field Emission Scanning Electron Microscopy

The FESEM technology provided the direct observation of Alumina nanofibres coated membrane, the surface morphology of the original support and the silane-grafted alumina nanofiber membrane is shown in Figure 3.7. The surface of porous support is rather rough with large pores of micron-scale. After coated with nanofibers on the surface, the support has been completely covered with fibers even though topography of the original support can still be identified. The enlarged image locally showed further the well-dispersed fiber layer on the surface. The alumina nanofiber layer has dramatically reduced the pore size of the resultant membranes without any obvious pin-holes and cracks.

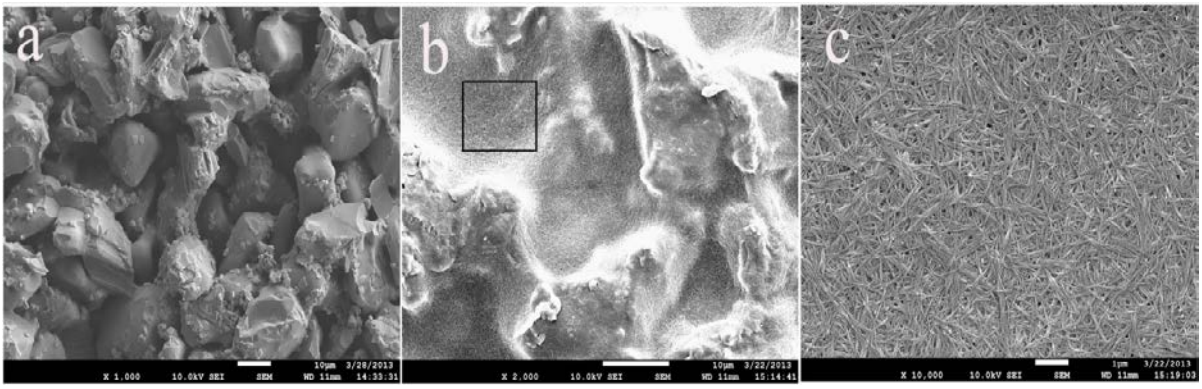

Fig. 3.7 FESEM images of the membrane surface of (a) a porous α-alumina support, (b) a silane-grafted fiber membrane, and (c) the enlarged image in the local area of (b).

3.3.3.5 Contact angle analysis

As shown in Figure3.8, it is the picture of a water drop on the surface of Al-membrane and NH-membrane. To compare the wetting property of the membranes, the contact angles of a blank support and a silane-grafted fiber membrane were measured. The contact angle for

Al-membrane is only is 16^{o} which indicates the hydrophily of the membrane surface. The results indicate that surface modified membranes present high hydro-phobicity. In the contrast, when water was dropped on the Al-membrane, it was instantly adsorbed by the membrane and left no drop on the surface. In contrast, after grafting with the silane groups, the contact angle increased to 136^{o} indicating highly hydrophobic surface was achieved after treatment. The contact angle analysis results illustrated that the APTES group has been successfully grafted on the Al-membrane and modified it from hydrophilic to high hydrophobic.

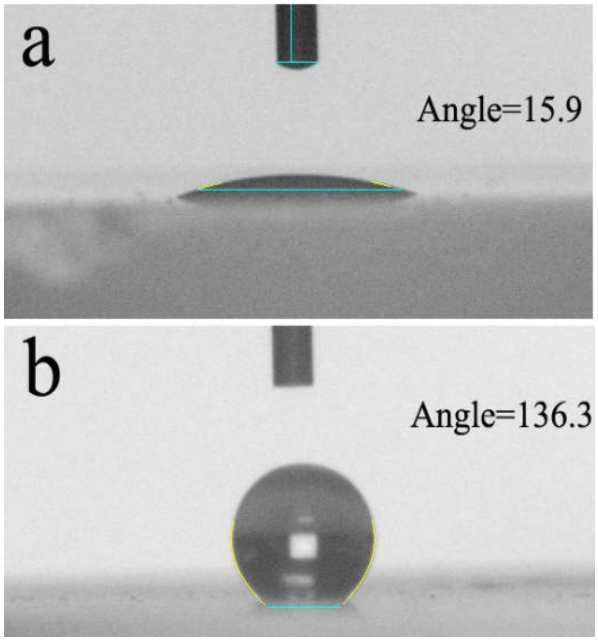

Figure 3.8 The contact angle of (a) a porous α-alumina support and (b) a silane-grafted fiber membrane.

3.3.3.6 FTIR spectrum

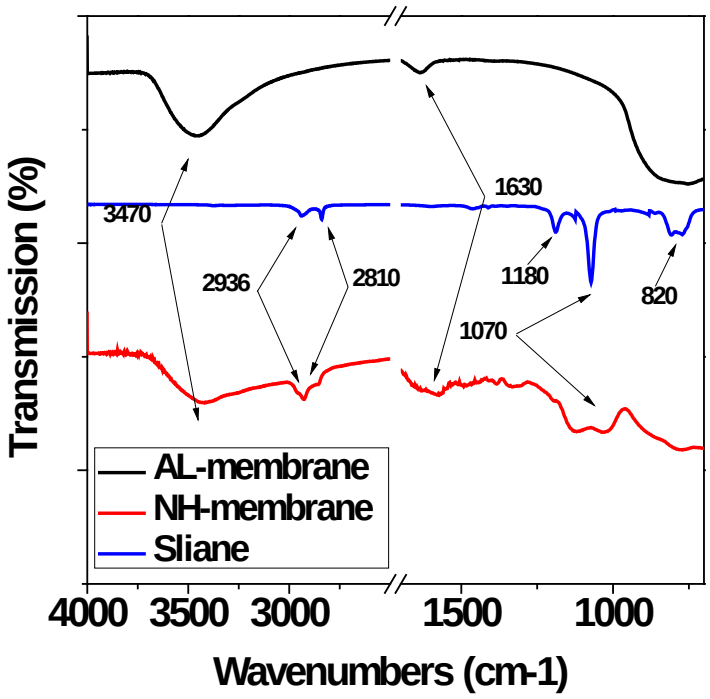

Figure 3.9 The FTIR spectra of Al-membrane, Silane(ApTES) and NH-membrane

Figure 3.9 shows the infrared spectra of alumina nanofiber membranes. The amounts of alumina fibers grafted on the surface of the support are very small, relative to the background of the Al-membrane. Thus, the samples were collected by scratching the surface of a silane-grafted fiber membrane and pressed the collected powders into a KBr pallet. The bands at 2861 cm^{-1} and 2925 cm^{-1} correspond to the $–CH_2–$ asymmetrical and symmetrical stretching vibrations of APTES (Fig.4c). The bands at 1027 and 1120 cm^{-1} represent the Si-O-C vibrations in APTES [36,37]. Thus, FTIR spectra confirmed the silane groups were grafted on the surface of fiber membranes.

3.3.4 Performance of Ultra-filtration Membrane

3.3.4.1 Pure water flux

To evaluate water permeability of the membranes, the pure water flux was measured at applied pressures. The water flux is determined by the equation $J_w = Q/(AT)$, where J_w is the pure water flux ($Lm^{-2}h^{-1}$), Q is the volume of water permeated (L), A is the effective membrane area (m^2), and T is the sampling time (h). Figure 6 shows the water flow rates through the membranes as a function of applied pressure. Pure water fluxes are proportional to the applied pressure for all these membranes. The porous support exhibited a high water permeability, approaching 800 $L \cdot h^{-1} \cdot m^{-2} \cdot bar^{-1}$. After the supports were coated with the nanofibers on the surface, the flux reduced to approximate 400 $L \cdot h^{-1} \cdot m^{-2} \cdot bar^{-1}$. When the silane groups were grafted on the surface of nanofiber membranes, the surfaces were modified to have a hydrophobic property, and thus the water flux was reduced by an order of magnitude up to 50 $L \cdot h^{-1} \cdot m^{-2} \cdot bar^{-1}$. The water flux curves were computationally extrapolated to zero flow rate, consequently the corresponding pressure of porous support, coated membrane and silane grafted membrane are 0.04bar, 0.05bar and 0.2 bar, the calculated results indicate the applied pressure where first permeation occurs. The relationship of applied pressure and effective radius is stated by Young-Laplace equation:

$$\Delta P = \frac{2\gamma \cdot \cos\theta}{r}$$

Where ΔP is the applied pressure, γ is the interfacial tension of water and air, θ is the wetting angle and r is the effective radius.

The changes of pure water fluxes may be largely attributed to the changes in pore size of the resultant membranes and the hydrophobic surface also plays a significant role.

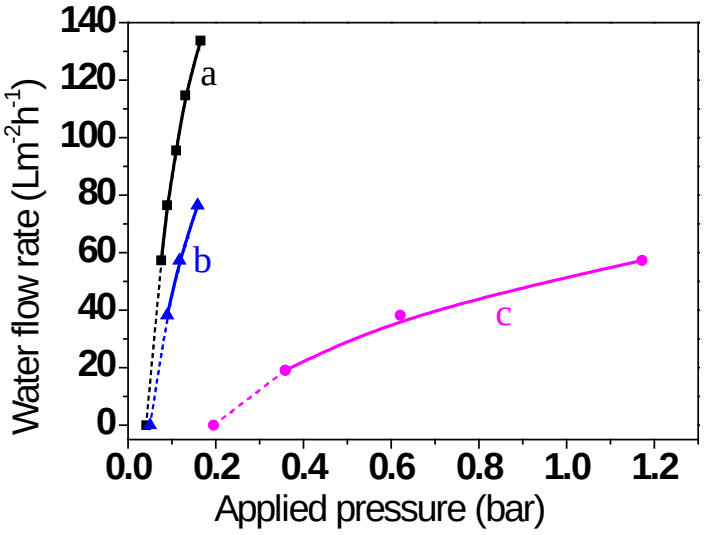

Figure 3.10 Water flow rates through membranes as a function of applied pressure: (a) a porous α-alumina support; (b) a γ-alumina fiber membranes and (c) a silane-grafted fiber membrane.

3.3.4.2 Pore-size Distributions and Dextran Retention Efficiency

The pore size distributions and separation efficiency of the membranes were tested and the results are displayed in Figure 3.11. The pore size distribution of the original porous support is centered on 700 nm (with the pore radius shown on the Figure 3.11 A). It has been remarkably improved by adding a nanofiber layer. Al-membranes

have pore sizes around 11 nm, similar with those of silane-grafted fiber membranes .

The separation efficiency of the membranes were tested by dextran retention test, the results are displayed in Figure 3.11 B. It can be found that the very low separation efficiency of original disc support had been remarkably improved by the boehmite nanofibres layer.

Based on the equation which indicates the relation between the molecular radius and molar mass:

$$A=0.33\cdot M^{0.46}$$

Where A is the molecular radius in Å and M is the molar mass of dextran in gram [46]. It can be calculated that the diameter of dextran of molecular weight 10K is 4.5nm. 40K is 8.6nm, 70K is 11 nm and 500K is 28nm. The molecular weight corresponding to dextran which rejection is over 90% is considered to be the cut-off molecular weight of the membrane.

According to the Figure 3.11 B, it can be found that Al-membrane exhibits a high rejection to the dextran of molecular weight 70K, the ratio reached 91%. The diameter of 70K is 11nm which means the pore size of Al- membrane is approximately 11nm. In addition, even through the performance of Al-membrane is higher than Bo-membrane when rejecting larger dextran molecular, however Bo-membrane exhibits better performance when rejecting 10K dextran. Bo-membrane and Al-membrane basically share the same surface morphology which explains their performances are generally similar,

however the residual organic surfactant on the boehmite nanofibres was contribute to the adsorption of small dextran on the membrane surface, this causes Bo-membrane rejected more 10K dextran than Al-membrane.

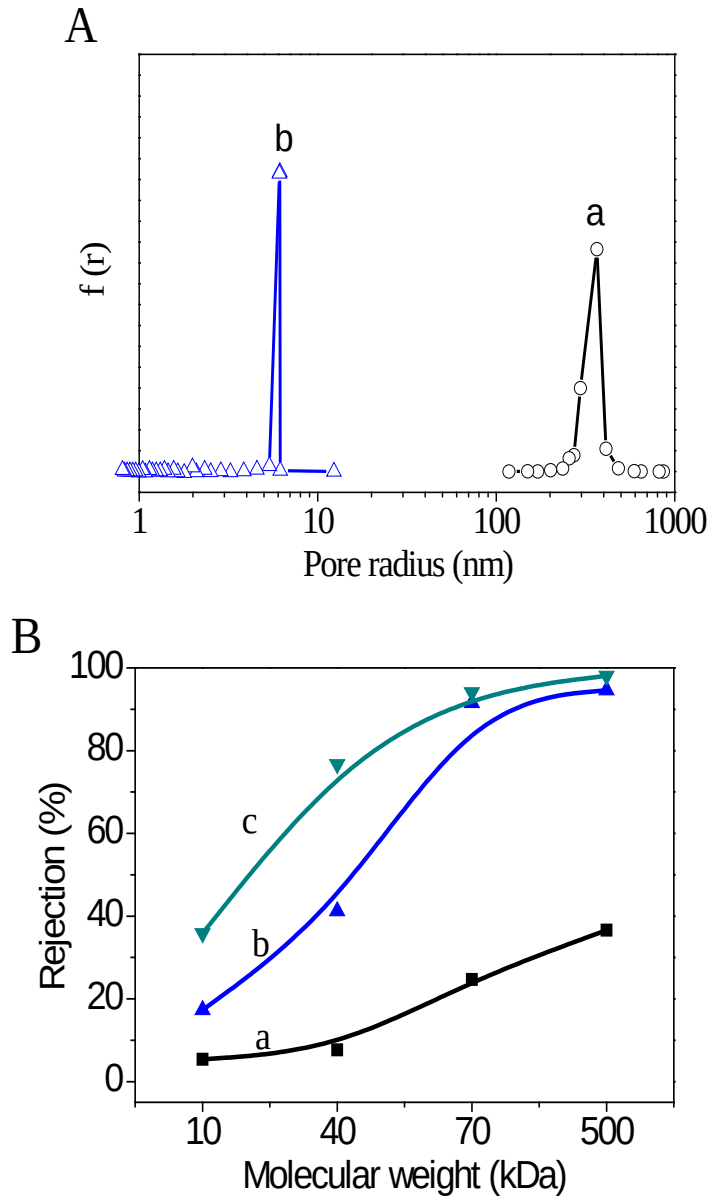

Fig. 3.11. *(A) Pore size distributions of various membranes: (a) a porous α-alumina support and (b) a γ-alumina fiber membrane. (B) Retentions of dextrans by gel permeation chromatography with different membranes. (a) a porous α-alumina support (b) a γ-alumina fiber membrane and (c) a silane-grafted fiber membrane.*

3.3.4.3 Protein Separation Efficiency

BSA (M.W. 66K Da), Cellulase (M.W. 45K Da) and Trypsin(M.W. 23.8K Da) were introduced into to protein separation test. The test results are shown in Figure 3.12. By comparing Figure 3.12 (a) (b) and (c), it can be found that all membranes exhibits better separation efficiency when the concentration of protein solution is low. The protein deposition and physical adsorption of membrane are the main reason to this phenomenon.

The Figure 3.12 (a) displays the rejection efficiency of membranes to BSA protein which has the largest molecular weight. The result indicates that blank support has very little rejection to BSA at all concentration range, the rejecting ability has been improved when Alumina nanofibres was coated. However, the rejection efficiency of Al-membrane to BSA is dramatically lower than to 70K dextran, given their molecular weight are close. Dislike the single dimension chain structure of dextran molecular, the peptide chain of protein molecular was spatially overlapped and turned to stereo structure. Because of this, the BSA molecular is smaller than 70K dextran molecular even through their molecular weight are similar. The NH-membranes on the other hand exhibits remarkable rejecting ability to BSA protein, the rejection ratio is close to 100%, it indicates that the hydrophobic modification has significantly increased the performance of Al-membrane due to the soluble protein are hydrophily and would be rejected by hydrophobic group.

The Figure 3.12 (b) and (c) are the results of the separation efficiency test using Cellulase and Trypsin. The data of these two tests theoretically matched the result of BSA test only except the separation efficiency is decreasing with the molecular weight decrease which is indicated in Figure3.12 (c). From Figure 3.12 (c), it can be found that NH-membrane almost rejects all the BSA protein and it is able to reject 92% of the Cellulase, however 45% of Trypsin can penetrate NH-membrane due to the smallest molecular weight and size.

To sum up, due to the size exclusion, the Al-membrane is able to reject all three proteins to a certain extent. When the surface of Al-membrane was modified to hydrophbicity, the separation efficiency had been significantly improved, the protein around 40K Da could be hold to the filtrate side. However, because of the approximately 10nm pore size, the Al-membrane is not able to reject protein corresponding to 23K Da even the hydrophobic group had been grafted on the surface.

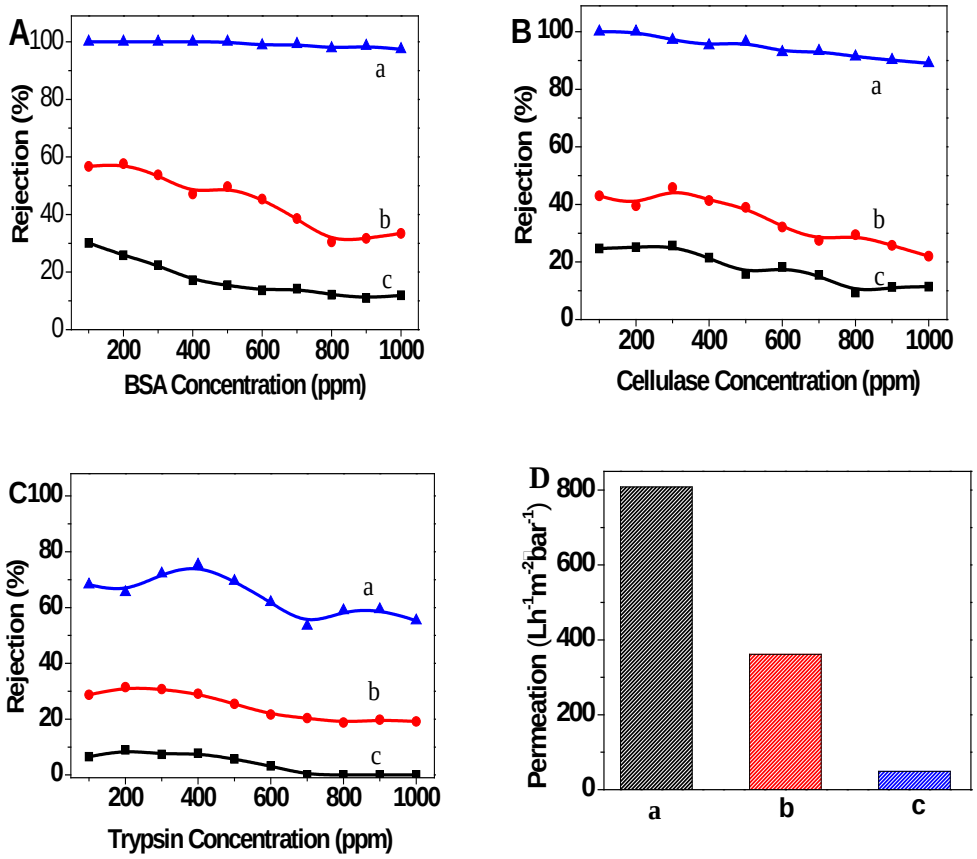

Figure 3.12 Protein separation efficiency of membrane. (a) BSA separation efficiency of membranes, (b) Cellulase separation efficiency of membranes, (c) Trypsin separation efficiency of membranes. (d) The permeation fluxes for various membranes.

3.4 CONCLUSION

The boehmite nanofibres was synthesised by hydrothermal reaction of aluminium hydrate cake in the presence of surfactant. The prepared boehmite nanofibres were approximate 100nm in length and 8-10nm in width. The boehmite nanofibres was attached on the surface of disc support by dip-coating and then sintered to convert to γ-Alumina phase, the attachment was confirmed by XRD analysis. APTES group was grafted upon the surface of alumina nanofiber layer and modified the surface to hydrophobicity property. The surface modification with silane grafting was confirmed by FTIR spectra and acontact angle analysis.

The size distribution characterization indicated that the high permeate efficiency of γ-alumina fiber membrane (as well as silane-grafted fiber membrane) with an average pore size of about 11nm. Water flux of membranes were measured to show the permeability, then dextran of different molecular weight was introduced to test the molecular cut-off of the prepared membrane, the result also indicates that the average pore size of Al-membrane is 11nm. The membranes showed excellent separation efficiency with the MWCO of 70 kDa and a permeation flux of 360 $L \cdot h^{-1} \cdot m^{-2} \cdot bar^{-1}$.

Proteins BSA, cellulase and trypsin were employed in the test of protein separation. The silane-grafted alumina fiber membrane was demonstrated to reject 100% BSA proteins and 92% cellulase. It can also retain 75% trypsin at the concentration of 400 ppm and maintain a permeation flux of 48 $L \cdot h^{-1} \cdot m^{-2} \cdot bar^{-1}$. The research progress should be of significance for the development of

new materials in membrane science and protein engineering. This study indicates that the great potential of ceramic nanofiber membranes for the real application of protein separation in terms of high flux, prominent selectivity and feasible surface modifications.

Chapter 4: Conclusion and Future Prospective

4.1 LACCASE IMMOBILISATION ON FUNCTIONALISED ALUMINA NANOFIBRES

The Boehmite nanofibres were synthesized using hydrothermal method and converted to γ-Alumina nanofibres. Alumina nanofibres of 80-120nm length and 10nm width were prepared for laccase immobilisation support. In the immobilisation section, the Alumina nanofibres were firstly grafted with APTES, the silane with an amino end. The cross linking agent Glutaraldehyde was introduced to link amino end and target laccase molecular, as a consequence, laccase was covalently immobilised on the surface of functionalised Alumina nanofibres. Characterisation techniques such as TEM, XRD and BET were employed to characterize the property of Alumina nanofibres and observe the morphology. The grafting of APTES functional group and the loading of cross linking agent was testified by IR spectra.

The immobilisation of laccase process had been studied on two main parameters and the optimized reaction condition for maximum immobilisation amount was determined. In addition, the original Alumina nanofibres which grafted ABTES only was applied in laccase immobilisation but using physical adsorption method, its results were compared to covalently immobilisation method.

ABTS was utilised as specific substrate to measure the catalytic activity. The activity tests indicated that most of the activity of laccase is retained after immobilisation process of both two methods. Additionally, for determine the resistant to environment change, the activity of immobilised laccase was tested in a range pH value and temperature, it was found that laccase exhibits better performance in low pH value and relatively high temperature environment, the results also indicates that immobilisation process has positive effect on the environment resistance. Finally, the constant cycle reaction test of immobilisation laccase was conducted in order to determine the reusability. Covalently immobilised laccase performance well in this test where physical adsorbed laccase almost complete lost its activity after 10 cycles of reaction.

Opportunities for future work in the laccase immobilisation on Alumina nanofibres could include novel reactor design for immobilised laccase and the practical application such as degradation of Phenolic compounds and pollutant water treatment.

4.2 FUNCTIONALISED ALUMINA MEMBRANE FOR PROTEIN SEPARATION

The fabrication of γ-Alumina nanofibres coated disc support was managed to form a new ultra-filtration system. The boehmite nanofibres was prepared by hydrothermal reaction of aluminium hydrogen gel in the presence of surfactant, the reaction temperature and period was optimised to be 130℃ and 48 hours to gain the balance of good boehmite crystal

structure and time efficiency. The prepared nanofibres were dip coated on the surface of disc support which exhibits very large water flux. Then the boehmite was heated to 550℃ in order to convert to γ-Alumina phase and sintered on the support surface. By grafting APTES group, the surface of coated disc support was modified to high hydrophobicity, the water flux of modified membrane was dramatically decreased.

The high-molecular polymer Dextran was employed to determine the molecular cut-off of the prepared ultra-filtration membranes, by utilizing the equation corresponding to the relation of molecular weight and size, the average pore size of Alumina nanofibres coated membranes was determined to be approximate 11nm. Finally, the protein separation test was conducted using three proteins of step down molecular weight, the surface modified ultra-filtration membrane exhibits expected performance in the test, it had been found to reject nearly 100% of BSA protein and 92% of cellulase molecular from water. However, due the limitation of the membrane, only 55% of Trypisn was rejected. To the future, more proteins of wide molecular rang could be introduced into the project and the performance of the ultra-filtration membrane could be tested in difference condition such as high temperature, extreme pH value and organic solvent.

Bibliography

1. Kuiry, S. C., E. Megen, et al. (2005). "*Solution-Based Chemical Synthesis of Boehmite Nanofibers and Alumina Nanorods*." The Journal of Physical Chemistry B 109(9): 3868-3872.

2. Shen, S. C., Q. Chen, et al. (2006). "*Steam-Assisted Solid Wet-Gel Synthesis of High-Quality Nanorods of Boehmite and Alumina*." The Journal of Physical Chemistry C 111(2): 700-707.

3. Shen, S.-C., W. K. Ng, et al. (2009). "*Solid-Based Hydrothermal Synthesis and Characterisation of Alumina Nanofibers with Controllable Aspect Ratios*." Journal of the American Ceramic Society 92(6): 1311-1316.

4. Liang, C. H., G. W. Meng, et al. (2001). "*Catalytic Growth of Semiconducting In2O3 Nanofibers*." Advanced Materials 13(17): 1330-1333.

5. Yu, H. and W. E. Buhro (2003). "*Solution–Liquid–Solid Growth of Soluble GaAs Nanowires*." Advanced Materials 15(5): 416-419.

6. Zhang, Z. and T. J. Pinnavaia (2002). "*Mesostructured γ-Al2O3 with a Lathlike Framework Morphology*." Journal of the American Chemical Society 124(41): 12294-12301.

7. Bugosh, J. (1961). "*Colloidal Alumina-The Chemistry and Morphology of Colloidal*." The Journal of Physical Chemistry 65(10): 1789-1793.

8. Lee, H. C., H. J. Kim, et al. (2003). "*Synthesis of Unidirectional Alumina Nanostructures without Added Organic Solvents*." Journal of the American Chemical Society 125(10): 2882-2883.

9. Zhu, H. Y., J. D. Riches, et al. (2002). "*γ-Alumina Nanofibers Prepared from Aluminum Hydrate with Poly(ethylene oxide) Surfactant*." Chemistry of Materials 14(5): 2086-2093.

10. Zhu, H. Y., X. P. Gao, et al. (2004). "*Growth of Boehmite Nanofibers by Assembling Nanoparticles with Surfactant Micelles*." The Journal of Physical Chemistry B 108(14): 4245-4247.

11. Claus, H. and Z. Filip (1997). "*The evidence of a laccase-like enzyme activity in a Bacillus sphaericus strain*." Microbiological Research 152(2): 209-216.

12. Baldrian, P. (2006). "*Fungal laccases – occurrence and properties*." FEMS Microbiology Reviews 30(2): 215-242.

13. Kirk, T. K., J. M. Harkin, et al. (1968). "*Degradation of the lignin model compound springgylglycol-β-guaiacyl ether by Polyporus versicolor and Stereum frustulatum*." Biochimica et Biophysica Acta (BBA) - General Subjects 165(1): 145-163.

14. Camarero, S., A. I. CaÑas, et al. (2008). "*p-Hydroxycinnamic Acids as Natural Mediators for Laccase Oxidation of Recalcitrant Compounds*." Environmental Science & Technology 42(17): 6703-6709.

15. Leonowicz, A., N. Cho, et al. (2001). "*Fungal laccase: properties and activity on lignin.*" Journal of Basic Microbiology 41(3-4): 185-227.

16. Mayer, A. M. and R. C. Staples (2002). "*Laccase: new functions for an old enzym*e." Phytochemistry 60(6): 551-565.

17. Annuar, M. S. M., S. S. Murthy, et al. (2010). "*Laccase production from oil palm industry solid waste: Statistical optimisation of selected process parameters*." Engineering in Life Sciences 10(1): 40-48.

18. Cho, S.-J., S. J. Park, et al. (2002). "*Oxidation of polycyclic aromatic hydrocarbons by laccase of Coriolus hirsutus*." Biotechnology Letters 24(16): 1337-1340.

19. Dai, Y., L. Yin, et al. (2011). "*Laccase-Carrying Electrospun Fibrous Membranes for Adsorption and Degradation of PAHs in Shoal Soils*." Environmental Science & Technology 45(24): 10611-10618.

20. Dhillon, G. S., S. Kaur, et al. (2012). "*Flocculation and Haze Removal from Crude Beer Using In-House Produced Laccase from Trametes versicolor Cultured on Brewer's Spent Grain*." Journal of Agricultural and Food Chemistry 60(32): 7895-7904.

21. Gitsov, I., J. Hamzik, et al. (2008). "*Enzymatic Nanoreactors for Environmentally Benign Biotransformations. 1. Formation and Catalytic Activity of Supramolecular Complexes of Laccase and Linear−Dendritic Block Copolymers.*" Biomacromolecules 9(3): 804-811.

22. Rodríguez Couto, S. and J. L. Toca Herrera (2006). "*Industrial and biotechnological applications of laccases: A review*." Biotechnology Advances 24(5): 500-513.

23. Shraddha, R. Shekher, et al. (2011). "*Laccase: Microbial Sources, Production, Purification, and Potential Biotechnological Applications*." Enzyme Research 2011: 11.

24. Durán, N., M. A. Rosa, et al. (2002). "*Applications of laccases and tyrosinases (phenoloxidases) immobilised on different supports: a review." Enzyme and Microbial Technology 31(7): 907-931.*

25. Wang, F., C. Guo, et al. (2008). "*Immobilisation of Pycnoporus sanguineus laccase by metal affinity adsorption on magnetic chelator particles.*" Journal of Chemical Technology & Biotechnology 83(1): 97-104.

26. Zheng, X., Q. Wang, et al. (2012). "*Biomimetic Synthesis of Magnetic Composite Particles for Laccase Immobilisation.*" Industrial & Engineering Chemistry Research.

27. Lloret, L., G. Eibes, et al. (2011). "*Immobilisation of laccase by encapsulation in a sol–gel matrix and its characterisation and use for the removal of estrogens*." Biotechnology Progress 27(6): 1570-1579.

28. Ma, H., P. Forssell, et al. (2011). "*Improving Laccase Catalyzed Cross-Linking of Whey Protein Isolate and Their Application as Emulsifiers*." Journal of Agricultural and Food Chemistry 59(4): 1406-1414.

29. Plagemann, R., L. Jonas, et al. (2011). "*Ceramic honeycomb as support for covalent immobilisation of laccase from Trametes versicolour and transformation of nuclear fast red."* Applied Microbiology and Biotechnology 90(1): 313-320.

30. Steffensen, C. L., M. L. Andersen, et al. (2008). "*Cross-Linking Proteins by Laccase-Catalyzed Oxidation: Importance Relative to Other Modifications*." Journal of Agricultural and Food Chemistry 56(24): 12002-12010.

31. Yinghui, D., W. Qiuling, et al. (2002). "*Laccase stabilisation by covalent binding immobilisation on activated polyvinyl alcohol carrier*." Letters in Applied Microbiology 35(6): 451-456.

32. Pita, M., C. Gutierrez-Sanchez, et al. (2011). "*High Redox Potential Cathode Based on Laccase Covalently Attached to Gold Electrode*." The Journal of Physical Chemistry C 115(27): 13420-13428.

33. Qiu, H., C. Xu, et al. (2009). "*Immobilisation of Laccase on Nanoporous Gold: Comparative Studies on the Immobilisation Strategies and the Particle Size Effects.*" The Journal of Physical Chemistry C 113(6): 2521-2525.

34. Vaz-Domínguez, C., M. Pita, et al. (2012). "*Combined ATR-SEIRAS and EC-STM Study of the Immobilisation of Laccase on Chemically Modified Au Electrodes*." The Journal of Physical Chemistry C 116(31): 16532-16540.

35. Zhu, Y., S. Kaskel, et al. (2007). "*Immobilisation of Trametes versicolor Laccase on Magnetically Separable Mesoporous Silica Spheres*." Chemistry of Materials 19(26): 6408-6413.

36. Liu, Y., Z. Zeng, et al. (2012). "*Immobilisation of laccase on magnetic bimodal mesoporous carbon and the application in the removal of phenolic compounds*." Bioresource Technology 115(0): 21-26.

37. Wang, Q., L. Peng, et al (2012). "*Fabrication of hydrophilic nanoporous PMMA/O-MMT composite microfibrous membrane and its use in enzyme immobilisation*." Journal of Porous Materials: 1-8.

38. Bayramoglu, G., I. Gursel, et al. (2012). "*Immobilisation of laccase on itaconic acid grafted and Cu(II) ion chelated chitosan membrane for bioremediation of hazardous materials*." Journal of Chemical Technology & Biotechnology 87(4): 530-539.

39. Bayramoglu, G., M. Yilmaz, et al. (2010). "*Preparation and characterisation of epoxy-functionalised magnetic chitosan beads: laccase immobilised for degradation of reactive dyes*." Bioprocess and Biosystems Engineering 33(4): 439-448.

40. Moccelini, S. K., A. C. Franzoi, et al. (2011). "*A novel support for laccase immobilisation: Cellulose acetate modified with ionic liquid and application in biosensor for methyldopa detection.*" Biosensors and Bioelectronics 26(8): 3549-3554.

41. Chen, J. H., Q. L. Liu, et al. (2007). "*Pervaporation and characterisation of chitosan membranes cross-linked by 3-aminopropyltriethoxysilane*." Journal of Membrane Science 292(1–2): 125-132.

42. Chang, M. C. and J. Tanaka (2002). "*FT-IR study for hydroxyapatite/collagen nanocomposite cross-linked by glutaraldehyde*." Biomaterials 23(24): 4811-4818.

43. Mansur, H. S., C. M. Sadahira, et al. (2008). "*FTIR spectroscopy characterisation of poly (vinyl alcohol) hydrogel with different hydrolysis degree and chemically crosslinked with glutaraldehyde*." Materials Science and Engineering: C 28(4): 539-548.

44. Johannes, C. and A. Majcherczyk (2000). "*Laccase activity tests and laccase inhibitors*." Journal of Biotechnology 78(2): 193-199.

45. Xu, F. (1996). "*Oxidation of Phenols, Anilines, and Benzenethiols by Fungal Laccases: Correlation between Activity and Redox Potentials as Well as Halide Inhibition*." Biochemistry 35(23): 7608-7614.

46. Wolfenden, B. S. and R. L. Willson (1982). "*Radical-cations as reference chromogens in kinetic studies of ono-electron transfer reactions: pulse radiolysis studies of 2,2[prime or minute]-azinobis-(3-ethylbenzthiazoline-6-sulphonate).*" Journal of the Chemical Society, Perkin Transactions 2(7): 805-812.

47. Ke, X. B., R. F. Shao, et al. (2009). "*Ceramic membranes for separation of proteins and DNA through in situ growth of alumina nanofibress inside porous substrates.*" Chemical Communications 0(10): 1264-1266.

48. Yang, D., B. Paul, et al. (2010). "*Alumina nanofibers grafted with functional groups: A new design in efficient sorbents for removal of toxic contaminants from water*." Water Research 44(3): 741-750.

49. Hildén, K., T. Hakala, et al. (2009). "*Thermotolerant and thermostable laccases*." Biotechnology Letters 31(8): 1117-1128.

50. Baldrian, P. (2004). "*Purification and characterisation of laccase from the white-rot fungus Daedalea quercina and decolorisation of synthetic dyes by the enzyme.*" Applied Microbiology and Biotechnology 63(5): 560-563.

51. Hublik, G. and F. Schinner (2000). "*Characterisation and immobilisation of the laccase from Pleurotus ostreatus and its use for the continuous*

elimination of phenolic pollutants." Enzyme and Microbial Technology 27(3–5): 330-336.

52. A.K. Pabby, S.S. H. Rizvi, A.M. Sastre, *Handbook of Membrane Separations: chemical, pharmaceutical, food, and biotechnological applications*, CRC Press, 2009.

53. J.C. Janson, *Protein purification: principles, high resolution methods, and applications*, 3rd edition, John Wiley & Sons, 2011.

54. R. van Reis, A. Zydney, *Bioprocess membrane technology*, J. Membr. Sci. 297 (2007) 16-50.

55. X. and E. Ruckenstein (1999). "*Membrane Chromatography: Preparation and Applications to Protein Separation*." Biotechnology Progress 15(6): 1003-1019.

56. M. Mahmoudi, I. Lynch, M. R. Ejtehadi, M. P. Monopoli, F. B. Bombelli, S. Laurent, *Protein-nanoparticle interactions: Opportunities and challenges*, Chem. Rev. 111 (2011) 5610-5637.

57. J. E. Rasmussen, C. B. Schiødt, S. F. Christensen, L. Nørskov-Lauritsen, M. Meldal, P. M. St Hilaire, K. J. Jensen, *Small-molecule affinity ligands for protein purification: Combined computational enrichment and automated in-line screening of an optically encoded library*, Angew. Chem. Int. Ed. 49 (2010) 3477-3480.

58. C. Casey, T. Gallos, Y. Alekseev, E. Ayturk, S. Pearl, *Protein concentration with single-pass tangential flow filtration (SPTFF)*, J. Membr. Sci. 384 (2011) 82-88.

59. Jungbauer, A. (2005). "*Chromatographic media for bioseparation*." Journal of Chromatography A 1065(1): 3-12.

60. Smejkal, G. B. (2005). *Separation Methods In Proteomics*. Hoboken, CRC Press.

61. Van Reis, R. and A. Zydney (2001). "*Membrane separations in biotechnology*." Current Opinion in Biotechnology 12(2): 208-211.

62. Mehta, A. and A. L. Zydney (2005). "*Permeability and selectivity analysis for ultrafiltration membranes*." Journal of Membrane Science 249(1–2): 245-249.

63. D. Yang, X. Niu, Y. Liu, Y. Wang, X. Gu, L. Song, R. Zhao, L. Ma, Y. Shao, X. Jiang, *Electrospun nanofibrous membranes: a novel solid substrate for microfluidic for microfluidic immunoassays for HIV*, Adv. Mater. 20 (2008) 4770-4775.

64. R.S. Barhate, S. Ramakrishna, *Nanofibrous filtering media: filtration problems and solutions from tiny materials*, J. Membr. Sci. 296 (2007) 1-8.

65. K. Yoon, K. Kim, X. Wang, D. Fang, B.S. Hsiao, B. Chu, *High flux ultrafiltration membranes based on electrospun nanofibrous PAN scaffolds and chitosan coating*, Polymer 47 (2006) 2434-2441.

66. S. Kaur, S. Sundarrajan, D. Rana, T. Matsuura, S. Ramakrishna, *Influence of electrospun fiber size on the separation efficiency of thin film*

nanofiltration composite membrane, J. Membr. Sci. 392-393 (2012) 101-111.

67. R. Wang, Y. Liu, B. Li, B. S. Hsiao, B. Chu, *Electrospun nanofibrous membranes for high flux microfiltration*, J. Membr. Sci. 392-393 (2012) 167-174.

68. 67 O.Kuttowy, S. S. (1975). "Cellulose *acetate ultrafiltration membrane*." J.Appl.Polym.Sci(19): 1449.

69. Sivakumar, M., D. R. Mohan, et al. (2006). "*Studies on cellulose acetate-polysulfone ultrafiltration membranes: II. Effect of additive concentration."* Journal of Membrane Science 268(2): 208-219.

70. Lv, C., Y. Su, et al. (2007). "*Enhanced permeation performance of cellulose acetate ultrafiltration membrane by incorporation of Pluronic F127*." Journal of Membrane Science 294(1–2): 68-74.

71. Zhao, W., Y. Su, et al. (2008). "*Fabrication of antifouling polyethersulfone ultrafiltration membranes using Pluronic F127 as both surface modifier and pore-forming agent*." Journal of Membrane Science 318(1–2): 405-412.

72. Arthanareeswaran, G., T. K. Sriyamuna Devi, et al. (2008). "*Effect of silica particles on cellulose acetate blend ultrafiltration membranes: Part I*." Separation and Purification Technology 64(1): 38-47.

73. Hester, J. F., P. Banerjee, et al. (1999). "*Preparation of Protein-Resistant Surfaces on Poly(vinylidene fluoride) Membranes via Surface Segregation*." Macromolecules 32(5): 1643-1650.

74. Yu, S., S. B. Lee, et al. (2001). "*Size-Based Protein Separations in Poly(ethylene glycol)-Derivatized Gold Nanotubule Membranes*." Nano Letters 1(9): 495-498.

75. Saxena, A., B. P. Tripathi, et al. (2009). "*Membrane-based techniques for the separation and purification of proteins: An overview*." Advances in Colloid and Interface Science 145(1–2): 1-22.

76. Van der Bruggen, B. (2012). "*The Separation Power of Nanotubes in Membranes: A Review."* ISRN Nanotechnology 2012: 17.

77. Li, J.-F., Z.-L. Xu, et al. (2009). "*Effect of TiO2 nanoparticles on the surface morphology and performance of microporous PES membrane*." Applied Surface Science 255(9): 4725-4732.

78. Soroko, I. and A. Livingston (2009). "*Impact of TiO2 nanoparticles on morphology and performance of crosslinked polyimide organic solvent nanofiltration (OSN) membranes.*" Journal of Membrane Science 343(1–2): 189-198.

79. Sotto, A., A. Boromand, et al. (2011). "*Doping of polyethersulfone nanofiltration membranes: antifouling effect observed at ultralow concentrations of TiO2 nanoparticles.*" Journal of Materials Chemistry 21(28): 10311-10320.

80. Yang, Y., H. Zhang, et al. (2007). "*The influence of nano-sized TiO2 fillers on the morphologies and properties of PSF UF membrane*." Journal of Membrane Science 288(1–2): 231-238.

81. Kim, J. and B. Van der Bruggen (2010). "*The use of nanoparticles in polymeric and ceramic membrane structures: Review of manufacturing procedures and performance improvement for water treatment*." Environmental Pollution 158(7): 2335-2349.

82. Rabiller-Baudry, M., B. Chaufer, et al. (2001). "*Ultrafiltration of mixed protein solutions of lysozyme and lactoferrin: role of modified inorganic membranes and ionic strength on the selectivity."* Journal of Membrane Science 184(1): 137-148.

83. Ke, X. B., Z. F. Zheng, et al. (2008). "*High-Flux Ceramic Membranes with a Nanomesh of Metal Oxide Nanofibers*." The Journal of Physical Chemistry B 112(16): 5000-5006.

84. Qiu, M., S. Fan, et al. (2010). "*Co-sintering synthesis of bi-layer titania ultrafiltration membranes with intermediate layer of sol-coated nanofibers*." Journal of Membrane Science 365(1–2): 225-231.

85. Ager, K., D. R. Latulippe, et al. (2009). "*Plasmid DNA transmission through charged ultrafiltration membranes*." Journal of Membrane Science 344(1–2): 123-128.

86. Calvo, J. I., et al. (2004). "Comparison of liquid–liquid displacement porosimetry and scanning electron microscopy image analysis to

characterise ultrafiltration track-etched membranes." Journal of Membrane Science 239(2): 189-197.